PFC/JA-86-29

CONVECTIVE INFLUX OF PLASMA AND BEAMS IN TOKAMAKS WITH AN ASYMMETRIC RIPPLE

T. F. Yang, P. W. Wang

March 1988

Convective Influx of Plasma and Beams in Tokamaks with an Asymmetric Ripple

T. F. Yang, P. W. Wang

Plasma Fusion Center
Massachusetts Institute of Technology
Cambridge, MA 02139 USA

Abstract

A method of inducing a convective influx of core plasma in tokamaks utilizing a specially structured vertical asymmetric ripple is proposed. In the ripple well the radial gradient of the toroidal field is increased on the flux surfaces in the plasma boundary layer below midplane. Also, the magnitude of the ripple decreases exponentially from the boundary toward the magnetic axis and is practically negligible above midplane. The guiding center orbit study demonstrates that counter-streaming circulating particles will drift toward the center due to extra inward drift from the increased gradient whenever the particle drifts through the ripple. The inward drift is manifested by $B \times \nabla B$ drift due to the increased length of the field line, and to slowing down and change of q values. Ripple trapped particles drift upward and become circulating or banana particles. The overall effect on the diffusion of banana particles is minimal. The influx is proportional to temperature and roughly to $(1 - \epsilon)$, where ϵ is the inverse aspect ratio. Due to this fact the enhancement of the penetration of beam injection can also be achieved by injecting the beam in the axisymmetric regions tangentially in the counter-streaming direction as well as injecting the beam perpendicularly into the ripple well.

1.0 Introduction

It has been pointed out by several authors [1-4] that there is an inward directed anomalous particle flux in tokamaks which is much greater than the Ware flux. The anomalous influx counteracts the diffusion and anomalous outflow and can give a proper explanation of the relatively peaked density profiles of tokamak devices. This paper discusses a method of inducing the influx by using a specially structured asymmetric ripple. The induced influx will also counteract the diffusion outflow like anomalous influx in a controlled fashion. This concept is intended as a means for particle control to reduce the flux to the divertor and limiter and to enhance the beam penetration. The known method of impurity and particle control in a tokamak is achieved by removing the particles via magnetic divertors or mechanical pumping limiters. In the divertor case the plasma in the scrape-off layer outside the separatrix is diverted away and dumped onto a remote target. The recycle will take place by allowing the neutral density to build up in the target chamber and near the edge of the plasma [5-11]. In the pumping limiter case the plasma in the boundary layer is dumped onto the limiter and recycling takes place due to the high density built up at the edge. In either case the impurities, as well as fuel particles, are recycled or pumped away through a vacuum system. However, there are many disadvantages and unresolved questions involved with these methods.

1. The fuel particles are recycled in an uncontrollable fashion, and impurities are recycled as well.
2. All diverted particles will first strike the target and/or limiter surfaces releasing large amounts of energy. The energy removal from the metal surfaces is difficult to handle. The surfaces will also be damaged due to erosion and sputtering which, in turn, generate metal impurities.
3. In order to maintain a reasonable vacuum, the particle throughput to the vacuum system requires very large, high speed vacuum pumps and a large duct area.

In this paper we propose to use local asymmetric ripple to drive some ions from the plasma edge into the center before they enter the scrape-off layer. Such a recycling method

will reduce the particle flux to the divertor target, limiter, and vessel wall, thus reducing the convective heat load and erosion on the wall surfaces and impurity generation.

The effect of ripple on particle orbits was studied in great detail, and it was found that a favorable drift could be obtained by optimizing the ripple characteristics. It is known that the peak of a ripple has an adverse effect on the confinement of banana orbits, particularly the effect of tip scattering [12,27]. Therefore it is quite obvious that one of the considerations is to minimize tip scattering by reducing the peak amplitude and increasing the well depth. Another consideration is to confine the ripple in a layer near the plasma boundary and construct the ripple in such a way that the gradient of the toroidal field is increased on the flux surfaces in the perturbed boundary layer. The increased gradient gives the particle an additional kick due to increased $\vec{B} \times \nabla \vec{B}/B^2$ drift when the particle passes through the ripple field. This extra inward movement is not compensated for in the axisymmetric region above the midplane, thereby resulting in a net inward drift. Such a ripple can be created by a set of pie-shaped coils whose plane is curved like the plasma boundary at a distance about one-third the plasma radius below the plasma boundary.

A modified Monte-Carlo guiding center code [28] was used to study the particle orbits. The particle orbits are no longer closed due to the presence of the ripple. The counter-streaming circulating and ripple trapped particles were drifting inward at a much higher speed than that of the co-streaming circulating particles. The drifting speed is proportional to particle energy. The drifting of banana orbits depends on the phase angle of the particles and on the region in which they are trapped. The net drift is very small in comparison with the circulating particle. However, collisions will cause some banana particles to become circulating particles; these would also drift inward. Therefore the overall diffusion of banana particles is not enhanced. The fraction of inwardly drifting particles without collision is proportional to $(1/2)(1 - \sqrt{\epsilon}) + (\Delta\phi/2\pi)\sqrt{\delta_0}$, where ϵ is the inverse aspect ratio, δ_0 is the ripple well depth and $\Delta\phi$ is the angular width of the ripple well measured from peak to peak. The influx was found proportional to $(1 - \epsilon)$, plasma temperature and an exponential function of (r/a) and inversely proportional to B_0 and charge.

Jassby and Goldston proposed to use asymmetric ripple as a means for enhancing

the penetration of beam injection [29]. A neutral beam was injected into the ripple well underneath the plasma. The beam ions drifted vertically into the center of the plasma and became banana particles. Perpendicular injection and an optimal injection energy of about 150 keV were required. From the drifting characteristics of the orbits we learned that enhancement of penetration could also be achieved by injecting the beam directly into the plasma tangentially outside the ripple in the counter-streaming direction. For the tangential injection the penetration speed increases with phase angle and energy. The penetration speed is a slow variation of phase angle; therefore, the beam divergency and orientation are not critical.

The ripple has little effect on the scraping off of energetic banana alpha particles; therefore the ash removal is not affected. The impurity generation is reduced due to the reduction of wall bombardment. Because of the high charge state of impurity ions, the influx of impurity is much lower than that of fuel ions.

The ripple characteristics and the method of ripple generation, a study of particle orbits, the effect on particle transport and an estimate of influx are discussed in detail in Sections 2, 3, and 4. Beam injection is discussed in Section 5.

2.0 Ripple Characteristics

The toroidal field in a tokamak with ripple, in general, can be written as

$$B_\phi = B_0 \left[\frac{R_0}{R} - \delta\left(r, \theta, \phi\right) \right]$$

or

$$B_\phi = B_0 \left(1 - \epsilon \cos\theta - \delta\left(r, \theta, \phi\right)\right) \ , \tag{1}$$

where $\epsilon = r/R$ is the ratio of the minor and major radii of the torus, δ is the ripple which is a function of the plasma radius, poloidal angle θ and toroidal angle ϕ. The periodical and vertically symmetric ripple caused by the discreteness of TF coils is usually in the form of [18,19]

$$\delta\left(r, \theta, \phi\right) = \delta_0 \left[r/a\right]^k \exp\left[-\left(\alpha\theta/\pi\right)^2\right] \cos N\phi \ . \tag{2}$$

where N is the number TF coils. The radial variation of $B(r,\theta,\phi)$ at the peak at $\phi = \pi/N$ and in the valley at $\phi = 0$ is typically like the solid curves in Fig. 1. The value of $\frac{\partial}{\partial R}B_\phi$ is reduced or even reversed at the peak and is increased in the valley. It is well known that the ripple of the form like Eq. (2) will enhance the diffusion and loss of energetic particles. This aspect has received substantial discussion by many authors [12-27]. However, very little attention has been paid to the local gradient in the ripple field.

The decreased radial gradient will reduce the vertical drift velocity proportional to $\vec{B} \times \nabla \vec{B}/B^2$ whereas increased gradient will increase the drift velocity. The vertical drift of a charged particle can be written as

$$\vec{v}_{dz} = \frac{1}{\Omega}\left(\frac{1}{2}v_\perp^2 + v_\parallel^2\right)\left[\frac{1}{R}\hat{z} + \frac{B_0}{B_\phi}\hat{b} \times \nabla\delta\right] . \tag{3}$$

The drift attributed to the change in gradient cancels out due to the rapidly oscillating nature of the ripple field and therefore does not contribute to diffusion to the first order. However, if the ripple well depth is much larger than the peak, the average gradient in the ripple will not cancel. The form of such a ripple can be written as

$$\delta(r,\theta,\phi) = \delta_0\left[\left(\frac{X+a}{2a}\right) + c\left(\frac{X+a}{2a}\right)^2\right]\left(\frac{r}{a}\right)^k \cdot \cos^m\left(\frac{\theta-\theta_0}{2}\right)\cos\left(\frac{\phi}{\lambda}\right)\exp\left[-\left(\frac{\phi}{\alpha}\right)^2\right] , \tag{4}$$

where $X = r\cos\theta$, c, λ, α, k, and m are constants determined by fitting this function with the field computed from a real coil configuration. The form of Eq. (4) was chosen such that the ripple is zero at $X = -a$. The coil configurations used to generate such a ripple are shown in Fig. 2. The ripple coil is located at a distance d from the bottom surface of the plasma. The angular separation of the radial conductor elements is $\Delta\phi$ which is approximately $2\pi/N$. The ripple is modeled based on a prototypical tokamak fusion reactor like INTOR [30] with plasma parameters $R_0 = 5.4$ m, $a = 1.6$ m, $k = 1.6$, $B_0 = 5.3$ T, $I_p = 7.5$ MA. The ripple coil is placed at 0.70 m from the surface and carries a current of 1 MA for an 8% ripple on the bottom of the plasma. The flux surfaces have been traced and were found to be nonergodic.

The vertical variation of the ripple is shown in Fig. 3, which shows that the ripple is largest at the bottom and decreases toward the midplane. The insert in the upper right corner shows the magnified ripple on the bottom line. It can be seen that the ripple well depth is much larger than the peak. Figure 4 plots the vacuum toroidal field along the perimeter of the plasma cross section below midplane. The dotted curve is a plot of the field at the peak of the ripple which shows that the gradient of B_ϕ in the major radial direction is decreased. The lower dashed curve is a plot of the field at the valley of the ripple well which shows that the gradient is increased. The perspective view of the field on the lower half of the plasma surface is shown in Fig. 5. The ripple well is like a trough. The contour plot of the ripple over the cross section of plasma in Fig. 6 shows that the ripple is not only confined below the midplane, but that is also concentrated near the surface; i.e., the ripple decreases radially from the surface toward the center of the plasma. The closest fitting of Eq. (4) to the toroidal field in Fig. 4 and to the ripple contour in Fig. 6 yields the values $\delta_0 = 0.1$, $c = 1.0$, $\lambda = 1/14.4$, $\alpha = 1/\sqrt{23.1}$, $m = 4$, $\theta_0 = -\pi/2$, and $k = 2$. The ripple at $\theta = -\pi/2$, $\phi = 0$ and $r = a$ is $\frac{3}{4}\delta_0 = 0.075$. The effect of this ripple on the particle orbits is discussed in the next section.

The coil set looks like a bundle divertor coil set [31] placed at the bottom. However, there are striking differences: There is a toroidal separatrix in the bundle divertor. The ripple is 100% at the null point and vertically symmetric. There is no separatrix in this case and the ripple is only 8%. The INTOR reactor was chosen for modelling to assure that the method is reactor applicable. The concept can be tested on an experimental device.

3.0 Particle Orbits

The particle orbits will be discussed in four classes: the trapped particles in the ripple well, the circulating particles, the deeply trapped banana particles below the peak at θ_2 (see Fig. 7), and the passing banana particles.

3.1 Ripple Trapped Particles

A typical ripple-trapped particle with an energy of 10 keV and $\chi = v_{\|}/v = 0.1$ launched in the ripple well at the bottom of the plasma is shown in Fig. 8. As previously predicted, the particle drifts upward toward the midplane and becomes a banana particle when it reaches the weak ripple region. The drifting velocity can be written as

$$\vec{v}_{dz} = \frac{\varepsilon}{M\Omega}\left[-\frac{1}{R}\hat{z} - \frac{B_0}{B_\phi}\hat{b}\times\nabla\delta\right] \ , \quad \chi \le \chi_{max} \ , \tag{5}$$

where ε is the kinetic energy and

$$\chi_{max} \le \sqrt{\delta_0} \ .$$

The penetration length is approximately

$$dz \approx a_0\left(1 - \frac{\chi^2}{\delta_0}\right) \ . \tag{6}$$

If the effective collision frequency ν_{eff}, $\nu_{eff} = \nu/\delta_0$, is greater than v_{dz}/dz, the penetration depth would be v_{dz}/ν_{eff}. Otherwise, the penetration depth will be determined by the ripple amplitude and the phase angle χ. The penetration depth as a function of χ is plotted in Fig. 9. The penetration is largest around $\chi = 0.0$ and is nearly zero when χ approaches $\chi_{max} \simeq \pm 0.27$.

3.2 Circulating Particles

The effect of the ripple on circulating particle orbits is different for counter-streaming and co-streaming particles. Particles of 3.5 MeV energy with $\chi = 0.8$ and -0.8 were launched at $\phi = 180°$ and $R = 680$ cm on midplane. The orbits were followed for ten turns around the torus and are shown in Figs. 10 and 11. The counter-streaming particle orbit drifts inward like a spiral. The co-streaming particle orbit drifts very little. The difference can be understood qualitatively from the following discussions. The drift velocity for the circulating particle in an axisymmetric tokamak is given as

$$v_{dz}^{s} = \frac{1}{2\Omega R_0}\left[2v_{\|}^2 + v_{\perp}^2\right] , \tag{7}$$

where the superscript s denotes the symmetric situation. The counter-streaming particle launched at midplane will move initially in the axisymmetric region above the midplane and drift upward at velocity v_{dz}^s. The maximum radial displacement for an axisymmetric torus can be calculated from

$$\Delta r = \int_0^{\pi q R} v_{dz}^s \sin\theta \frac{d\ell}{v_\parallel}$$

which is approximately

$$\Delta r \simeq \int_0^\pi \frac{1}{2\Omega R_0}\left(2v_\parallel^2 + v_\perp^2\right)\frac{\sin\theta}{v_\parallel} qR d\theta$$

$$= \frac{2}{\Omega}\frac{q(r)}{2v_\parallel(0)}\left\{2v_{\parallel,\pi}v_{\parallel,0}\left(1+\frac{11}{8}\frac{1}{v_\parallel(0)^2}\frac{2\mu B_0}{M}\epsilon\right)\right.$$

$$\left. + v_\perp^2\left[1+\frac{3}{24}\left(\frac{3\mu B_0\epsilon}{M v_\parallel(0)}\right)^3\right]\right\}, \tag{8}$$

where $v_\parallel(0) = v_\parallel(r=0)$ is the averaged parallel velocity

$$v_\parallel(0) = \sqrt{\frac{2}{M}(\varepsilon - \mu B_0)}\,|_{R=R_0} \ , \tag{9}$$

$v_{\parallel,0} = v_{\parallel,0}(r=a,\theta=0)$ is the parallel velocity at $\theta = 0°$ on the midplane

$$v_{\parallel,0} = \sqrt{\frac{2}{M}(\varepsilon - \mu B_0 + \mu B_0\epsilon)} \ , \tag{10}$$

and $v_{\parallel,\pi} = v_{\parallel,\pi}(r=a,\theta=\pi)$ is the parallel velocity at $\theta = 180°$ on the midplane

$$v_{\parallel,\pi} = \sqrt{\frac{2}{M}(\varepsilon - \mu B_0 - \mu B_0\epsilon)} \ . \tag{11}$$

When the particle travels below the midplane it will drift upward toward the midplane with v_{dz}^s and receive an additional kick from $\nabla\delta$ when it passes through the ripple. As will be discussed later, this extra drift causes the orbit to be displaced by δr inwardly on the midplane at $\theta = 0°$, instead of remaining a closed orbit as in the axisymmetric toroidal field case. The extra displacement reduces the inverse aspect ratio ϵ, which becomes $\epsilon' = (r - \delta r)/R_0$. The particle is now drifting on the inner flux surface which has a lower

q value. As seen from Eq. (8) both of these changes will reduce Δr on the upward drift of each turn. Therefore, the orbit is seen to be spiraling inward. On the other hand, the co-streaming particle will initially travel downward below midplane and drift inward with v_{dz}^s. The orbit will be displaced by Δr inwardly from the plasma surface. Therefore, the particle will pass through a much weaker ripple region and the additional kick due to the ripple is much less. There are many other factors that contribute to the nonequal drifting of the counter-streaming and co-streaming circulating particles. A qualitative discussion is given below.

Figure 12 plots the toroidal field along the counter-streaming and co-streaming orbits as a function of time. The counter-streaming particle passed the ripple at about $\theta = -\pi/2$ where the ripple amplitude is largest. The co-streaming particle passed the ripple near $\theta = -\pi/4$ on the inner surface where the ripple amplitude is much smaller. As can be seen from Eqs. (10) and (11), the parallel velocity $v_{\|}$ of counter-streaming circulating particles is smaller than that of co-streaming particles because it is traveling on a surface with a larger aspect ratio; thus the traveling time is longer. The poloidal drift velocity, due to a radial component of the ripple field, changes direction for the two types of particles and would give rise to different effects on their radial drifts. The counter-streaming particle always drifts toward the ripple from the high field side shown by the downward arrow in Fig. 12. The gradient along the field line is $\frac{\partial B_\phi}{\partial \ell} = B_0 \epsilon \sin\theta / qR$ which is positive above midplane and negative below midplane. The radial field B_r due to the ripple is negative before the particle reaches the peak at θ_1. Therefore, the poloidal drift velocity, which is proportional to $\vec{B}_r \times \overrightarrow{\partial B_\phi} / \partial \ell$, is positive. This means that poloidal drift of the orbit is in the decreasing $|\theta|$ direction which enters a region where the ripple and gradient are increasing. The situation is reversed for co-streaming particles because B_r is negative when the particles approach the peak at θ_2 from the low field side indicated by the upward arrow in Fig. 12. Now the poloidal drift is negative and the particle would drift in the increasing $|\theta|$ direction into a decreasing ripple region. There is a toroidal drift velocity $v_{d\phi}^s$, proportional to $\vec{B}_p \times \overrightarrow{\partial B_\phi} / \partial R$. The impact of this drift velocity on the radial drifts of the two types of particles depends on the region in which the particles are traveling.

In the quadrant $(0 > \theta > -\pi/2)$ the drift velocity $v^s_{d\phi}$ is in the co-streaming direction; therefore, the parallel velocity of the counter-streaming circulating particle is reduced and that of the co-streaming particles is increased. The effect is the opposite in the quadrant $(-\pi/2 > \theta > -3\pi/2)$. However, the slowing down in time would contribute more to the inward drift in the first quadrant where the ripple is larger. The effects from all these factors just described are cumulative and are difficult to illustrate separately. Nonetheless, it is quite clear that the combined results of these factors would make the inward drift of the counter-streaming circulation particles larger than that of the co-streaming particles.

Besides the inward kick on the particle due to the increased gradient in the ripple well, there is an additional contribution to the inward displaement from the axisymmetric drift velocity v^s_{dr} due to the increase in the length of the field line $d\ell$ and change of q value. The evaluation of $d\ell$ is carried out below.

The divergence-free magnetic field can be written as

$$\vec{B} = \frac{B_0}{1+\epsilon\cos\theta}\left\{\frac{B_r(r,\theta,\phi)}{B_0}\ ,\ \frac{\epsilon}{q}\ ,1-(1+\epsilon\cos\theta)\delta(r,\theta)\cos\left(\frac{\phi}{\lambda}\right)\exp\left[-\left(\frac{\phi}{\alpha}\right)\right]^2\right\} \quad (12)$$

and

$$B_r(r,\theta,\phi) = -B_0\epsilon\delta(r,\theta)\kappa(r,\theta)f(\phi)\ , \quad (13)$$

where

$$\delta(r,\theta) = \delta_0\left[\left(\frac{r\cos\theta+a}{2a}\right)+c\left(\frac{r\cos\theta+a}{2a}\right)^2\right]\left(\frac{r}{a}\right)^k\cos^m\left(\frac{\theta-\theta_0}{2}\right) \quad (14)$$

$$f(\phi) = \left[2\frac{\phi}{\alpha^2}\cos\left(\frac{\phi}{\lambda}\right)+\frac{1}{\lambda}\sin\left(\frac{\phi}{\lambda}\right)\right]\exp\left[-\left(\frac{\phi}{\alpha}\right)^2\right]\ , \quad (15)$$

$$\kappa = \frac{1}{\delta(r,\theta)}\int_0^{'}\chi\delta(\chi r,\theta)d\chi\ . \quad (16)$$

With some arithmetic and following Davidson's method [19] we can obtain

$$\frac{d\ell}{d\theta} = \left(1-\delta(r,\theta)\cos\left(\frac{\phi}{\lambda}\right)\exp\left[-\left(\frac{\phi}{\alpha}\right)^2\right]-Qq\int_0^{\theta}\delta(r,\theta')\kappa(r,\theta')f(q(\theta'-\theta_0))d\theta'\right)q(r_0)R \quad (17)$$

where

$$Q = \frac{d\ell nq}{d\ell nr} \ . \tag{18}$$

The radial drift velocity including ripple is

$$\begin{aligned} v_{dr} &= \frac{1}{2\Omega R_0}\left(2v_\parallel^2 + v_\perp^2\right)\left(1 + R_0\frac{d\delta}{dR}\right)\sin\theta \\ &= v_{dr}^s + v_{dr}^r \ . \end{aligned} \tag{19}$$

Here the axismmyetric drift and the drift due to ripple gradients are respectively

$$v_{dr}^s = \frac{1}{2\Omega R_0}(2v_\parallel^2 + v_\perp^2)\sin\theta \ , \quad v_{dr}^r = \frac{1}{2\Omega}\left(2v_\parallel^2 + v_\perp^2\right)\frac{d\delta}{dR}\sin\theta \ . \tag{20}$$

For traveling one revolution around the torus the inward deviation at midplane due to ripple is

$$\begin{aligned} \delta r &= \oint v_{dr} d\ell / v_\parallel \\ &= +\frac{1}{M\Omega R_0}\oint\Bigg\{\left[Mv_\parallel + \mu B\frac{1}{v_\parallel}\right]R_0\frac{d\delta}{dR}\sin\theta \\ &- \left[Mv_\parallel + \mu B\frac{1}{v_\parallel}\right]\delta(r,\theta)\sin\theta\cos\left(\frac{\phi}{\lambda}\right)\exp\left[-\left(\frac{\phi}{\alpha}\right)^2\right] \\ &- Qq\left[Mv_\parallel + \mu B\frac{1}{v_\parallel}\right]\sin\theta\int_0^\theta \delta(r,\theta')\kappa(r,\theta)f(q(\theta'-\theta_0)d\theta'\Bigg\}q(r_0)Rd\theta \ , \end{aligned} \tag{21}$$

where only the first order terms are retained and the axisymmetric term vanishes. The first term is the extra drift due to the ripple gradient. The approximate value of δr for a field pasing through $r = a$ $\theta = -\pi/2$ and $\phi = 0°$ is

$$\delta r \simeq -\left(\frac{Mv_\parallel^2(0) + \mu B_0}{M\Omega v_\parallel(0)}\right) \times \frac{\pi q(r_0)\delta_0}{2}\left(\frac{R_0}{a} + \frac{3}{4} + \frac{3}{v}Q\right) \tag{22}$$

It can be seen here that the axisymmetric drift velocity gives additional inward displacement due to the change of length in the second term and the change in the value of q in the third term. The change of $q(r)$, Q, near the boundary surface is very steep,

especially when the separatrix is present. Therefore, these two contribution to the inward displacement can be significant.

The normal negative main ion pressure gradient ($p' < 0$) produces a negative contribution ($E_r < 0$) to the radial electric field. The ripple induced influx contributes a positive component to the radial electric field ($\Delta E_r > 0$). Therefore, the ambipolar electric field set up by diffusion processes will be reduced and the poloidal rotation frequency, $\omega_E = E_r/rB$, becomes smaller. Ten keV particles' orbits are tested by using the radial electric field, $E_r = \pm\nabla p/ne$. The poloidal rotation drift due to the radial electric field quickly causes the ripple trapped particles to become detrapped. However, it has little effect on the circulating particles which dominate the inflow process.

3.3 Banana Orbits

The effect of ripple on the banana orbits can be discussed in three regions as shown in Fig. 7. The first region is where the bananas are trapped below the peak at θ_2. The second region is between peak at θ_1 and θ_2. The third region is above the peak at θ_1.

In region 1, the effect of the change of gradient on the confinement of banana particles can be roughly estimated following Yushmanov's method [24]. The deceleration of the banana tip near θ_2 is

$$\frac{dv_\parallel}{dt} = \frac{v_\perp^2}{2}\left(\frac{\epsilon}{qR}\sin\theta - \frac{d\delta}{d\ell}\right) \tag{23}$$

To drastically simplify the problem, let us consider the field line passing through $r = a$, $\theta = -\pi/2$, $\phi = 0°$. The field equation is $\theta = \phi q = \pi/2$ and $\ell = qR\theta$. The banana would bounce back and forth between $\theta_2 = \phi_2/q - \pi/2$ and $\theta_2' = -\phi_2/q + \pi/2$ as shown in Fig. 7, where $\phi_2 = 1/2\Delta\phi \simeq \pi/2N$. The length of this segment of field line is $d\ell \simeq R\pi(q - 2/N)$. Using the ripple equations (4), (14), and (15) and approximating $\cos\theta_2 \simeq 0$ and $\sin\theta_2 = 1$, the deceleration is reduced to

$$\frac{dv_\parallel}{dt} \simeq \frac{v_\perp^2}{2}\left[\frac{\epsilon}{qR} - 0.82\frac{\pi\delta_0}{R}\right]$$

The transit time for the banana below midplane is approximately

$$t_1 \simeq \sqrt{\frac{1}{2} qR\pi \Big/ \frac{dv_\parallel}{dt}}$$

$$\simeq \frac{qR}{v_\perp}\sqrt{\frac{\pi}{\epsilon}}\left[1 + 0.41\frac{q\pi\delta_0}{\epsilon}\right] \tag{24}$$

The transit time for the banana above the midplane is

$$t_2 = \frac{qR}{v_\perp}\sqrt{\frac{\pi}{\epsilon}} \tag{25}$$

The time difference is

$$\Delta t \simeq 0.41\left(\frac{\pi}{\epsilon}\right)^{3/2}\frac{Rq^2\delta_0}{v_\perp} \tag{26}$$

The total displacement can be written as

$$\delta r = v_{dr}^s \Delta t - v_{dr}^r \cdot t_1 \ . \tag{27}$$

The axisymmetric radial drift velocity v_{dr}^s is negative below the midplane. If the drift due to the ripple gradient v_{dr}^r is zero, the banana would actually drift inward. However, in region 1 the banana tip would encounter the peak at θ_2 and the additional drift v_{dr}^r due to ripple would also be negative. The displacement Δr is greater than zero when the second term dominates. Therefore, the banana would drift out horizontally like the orbits shown in Fig. 13.

In region 2, the tip of the banana orbit passes the peak at θ_2 and the valley of the ripple and then bounces off the peak at θ_1. The average v_{dr}^r is now positive; thus enhances the inward drift of the first term. The banana tip always drifts to the inner flux surface when it is bounced at θ_1. The tip keeps moving upward and continues drifting toward the inner surfaces. Such an orbit is shown in Fig. 14. A particle was launched at point 0 on the midplane and returned to a smaller radius at point f on the midplane after one bounce. Figures 15 and 16 are the result of multiple bounces for a banana with $\chi = \pm 0.50$. The upward drift of the lower tip causes the banana to move toward the inner flux surface. This banana orbit eventually becomes detrapped and continues the inward drift as a circulating

particle. In region 3, the averaged v_{dr}^{r} is reduced because of the negative ripple gradient of the peak at θ_1. The effect becomes insignificant when χ increases.

The diffusion coefficient for the banana particles should be evaluated separately for each region. The diffusion was enhanced in region 1 and reduced in regions 2 and 3. If the collision frequency ν is less than the bounce frequency ω_b, i.e., the banana is able to complete one bounce between collisions, then the overall diffusion coefficient can be written as the sum of three terms $D = \sqrt{\epsilon}(f_1(\Delta r + \delta r_1)^2 \nu_{eff1} + f_2(\Delta r - \delta r_2)^2 \nu_{eff2} + f_3(\Delta r - \delta r_2)^2 \nu_{eff3})$, where f_1, f_2, and f_3, are the fraction of particles trapped in each of the regions and their sum $(f_1 + f_2 + f_3)$ should be unity. The diffusion coefficient would reduce to $D = \sqrt{\epsilon}(\Delta r)^2 \nu_{eff}$ for an axisymmetric torus.

4.0 Particle Transport

To evaluate the overall effect of the asymmetric ripple on particle transport, the drift boundary in the velocity space was identified. To do so, particles of energy ranging from 0.05 keV to 3.5 MeV were launched on the midplane from a flux surface at radius $r_0 = 150$ cm and at $\phi = 180°$ and $\theta = 0°$. The particles were tracked either as they travelled past the ripple and completed one or several toroidal revolutions, or as they were reflected. The comparison of final radius r_f with initial radius r_0 was used to determine the inward or outward drift. Positive values of the radial difference $\Delta r = r_f - r_0$ gives outward drift and negative $\Delta r = r_f - r_0$ gives inward drift. There was no deviation in orbit when the particles were traveling in the axisymmetric region of the torus until they reached the ripple region. The slow-drifting bananas were launched at smaller toroidal angles in such a way that the lower tip began in the ripple free region. The final position r_f was also determined when the particle returned to the initial angular position ϕ_i if it was reflected by the ripple or to an angular position $-\phi_i$ if it had passed through the ripple. All the other bananas were followed for one complete revolution. The circulating particles were followed at least ten toroidal revolutions so that an averaged drift could be obtained.

The drifting boundaries are presented in Fig. 17. The shaded areas for χ in the domains $-0.22 \leq \chi \leq 0.22$ and $0.32 \leq \chi \leq 0.47$ are outward drifting banana regions. The

domains $-0.47 < \chi < -0.22$ and $0.22 < \chi < 0.32$ are inward drifting banana regions. The deviation of the co-streaming circulating particles from axisymmetric orbits is very small; therefore, the drift region cannot be clearly defined. The impact of the drifting regions on transport can be seen by the drifting speed plotted in Fig. 18. The net drift for the banana and co-streaming particles is nearly zero. Therefore the enhancement of diffusion coefficients from these particles appears to be small. The counter-streaming circulating particles drift inward at a much greater speed which increases with energy and χ. The effect of the collision on the orbits can be best demonstrated by Fig. 19. A 10 keV particle with $\chi = 0.30$ was launched inside the ripple. It was trapped initially and then, due to collision, became a banana orbit which is shown by the heavy curve in Fig. 19. Figure 20 shows the fluctuation of χ due to collisions. Again the banana orbit became circulating as a result of the collision. The circulating orbit travels inward despite the successive collisions indicated by the dashed curves.

The inflow flux can be developed by following Frieman's work [14]. Introducing the coordinates in velocity space $(v_\perp, v_\parallel, \zeta)$ by means of

$$\vec{v} = v_\parallel \vec{n} + v_\perp (\hat{e}_1 \cos\zeta + \hat{e}_2 \sin\zeta) \tag{28}$$

with

$$\vec{n} = \vec{B}/B \tag{29}$$

and $\mu = \frac{1}{2} v_\perp^2 / B$, $\varepsilon = \frac{1}{2}(v_\parallel^2 + v_\perp^2)$, with the inclusion of gradients of the ripple, the second order Fokker-Planck equation can be written as

$$\begin{aligned} & v_\parallel \vec{n}\cdot\nabla f_1 - \frac{e}{M}\vec{n}\cdot\nabla\Phi v_\parallel \frac{\partial f_1}{\partial\varepsilon} - \frac{e}{M}\vec{n}\cdot\nabla\Phi_1 v_\parallel \frac{\partial f_0}{\partial\varepsilon} \\ & + \vec{v}_\perp \cdot [\nabla f_1 - \left(\mu\nabla B + v_\parallel^2 \vec{n}\cdot\nabla\vec{n} - \frac{e}{M}\nabla\Phi\right)\frac{1}{B}\frac{\partial f_1}{\partial\mu} \\ & - (-\mu\nabla\delta B + v_\parallel^2 \vec{n}\cdot\nabla\vec{n}_\delta)\frac{1}{B}\frac{\partial f_0}{\partial\mu} - \frac{e}{M}\nabla\Phi\frac{\partial f_1}{\partial\varepsilon} - \frac{e}{M}\nabla\Phi_1\frac{\partial f_0}{\partial\varepsilon}] \\ & - v_\parallel \mu \frac{\partial f}{\partial\mu}[A] + \frac{\partial f_1}{\partial\zeta}[B] \\ & - \frac{e}{M v_\perp}\nabla\Phi\cdot(\hat{e}_2\cos\phi - \hat{e}_1\sin\phi)\frac{\partial f_1}{\partial\zeta} - \Omega\frac{\partial f_2}{\partial\zeta} \\ & = C(f_0, f_1) + C(f_1, f_0)\ , \end{aligned} \tag{30, 31}$$

where the coefficients A and B are defined in Reference 14. The Maxwellian f_0 and the first order function f_1 are given respectively as

$$f_0 = n(M/2\pi T)^{3/2} \exp(-M\varepsilon/T) \ , \tag{32}$$

and

$$f_1 = \overline{f}_1 + \tilde{f}_1 \tag{33}$$

with

$$\tilde{f}_1 = \frac{v_\perp}{\Omega}(\hat{e}_1 \sin\zeta - \hat{e}_2 \cos\zeta) \cdot \left(\nabla f_0 - \frac{e}{M} \nabla\Phi \frac{\partial f_0}{\partial \epsilon} \right) \ , \tag{34}$$

using the standard notation

$$\frac{\partial \overline{f}_n}{\partial \zeta} = 0 \ ; \quad \int_0^{2\pi} d\zeta \tilde{f}_n = 0 \ . \tag{35}$$

The continuity equation is

$$\frac{\partial n}{\partial t} + \nabla \cdot \int d^3 v \vec{v} f = 0 \ , \tag{36}$$

where

$$n(\psi) = n_0(\psi) \exp[-e\Phi(\psi)/T] \ . \tag{37}$$

Through second order, Eq. (36) becomes

$$\frac{\partial n_0}{\partial t} + \nabla \cdot \int \frac{B d\mu d\varepsilon d\phi}{|v_\parallel|} \left(v_\parallel \vec{n} + \vec{v}_\perp \right) f_2 = 0 \ . \tag{38}$$

Introducing the coordinates ψ, β, ϕ such that

$$\vec{B} = \nabla\psi \times \nabla\beta \ , \quad \beta = q\theta - \phi \tag{39}$$

and integrating (38) over θ and ϕ we have

$$\frac{\partial n_0}{\partial t} + \frac{\partial}{\partial \psi} \int \frac{d\theta}{2\pi} \frac{d\phi}{2\pi} \int \frac{B d\mu d\varepsilon d\zeta}{|v_\parallel|} \vec{v}_\perp \cdot \frac{\nabla\psi}{|\nabla\psi|} \tilde{f}_2 = 0 \ . \tag{40}$$

We obtain the integrand

$$
\begin{aligned}
I &= \int d\zeta \vec{v}_\perp \cdot \frac{\nabla\psi}{|\nabla\psi|}\tilde{f}_2 \\
&= -\int d\zeta v_\perp (\hat{e}_1 \sin\zeta - \hat{e}_2 \cos\zeta) \cdot \frac{\nabla\psi}{|\nabla\psi|}\frac{\partial \tilde{f}_2}{\partial\zeta} \\
&= \frac{v_\parallel^2}{2\Omega}\vec{n}\times\left(\nabla\tilde{f}_1 - \left(\mu\nabla B + v_\parallel^2 \vec{n}\cdot\nabla\vec{n} - \frac{e}{M}\nabla\Phi\right)\frac{1}{B}\frac{\partial f_1}{\partial\mu}\right. \\
&\left. - \left(-\mu\nabla\delta + v_\parallel^2\vec{n}\cdot\nabla\vec{n}_\delta\right)\frac{1}{B}\frac{\partial f_0}{\partial\mu} - \frac{e}{M}\nabla\Phi\frac{\partial\overline{f}_1}{\partial\varepsilon} - \frac{e}{M}\nabla\Phi_1\frac{\partial f_0}{\partial\varepsilon}\right) \\
&+ \frac{v_\perp}{\Omega}\int d\zeta\,(\hat{e}_1\sin\zeta - \hat{e}_2\cos\zeta)\left[C(f_0,\tilde{f}_1) + C(\tilde{f}_1,f_0)\right] \ . \qquad (41)
\end{aligned}
$$

Substituting this into Eq. (40) and carrying out the further integration by parts one can readily obtain

$$
\begin{aligned}
&\frac{\partial n_0}{\partial t} + \frac{\partial}{\partial\psi}\int\frac{d\theta}{2\pi}\frac{d\phi}{2\pi}\int\frac{B d\mu d\varepsilon 2\pi}{|v_\parallel|}\left[\vec{v}_{dz}^{\,s}\cdot\frac{\nabla\psi}{|\nabla\psi|}\overline{f}_1 + \vec{v}_{dz}^{\,r}\cdot\frac{\nabla\psi}{|\nabla\psi|}f_0\right] \\
&\quad + \frac{\partial}{\partial\psi}\int\frac{d\theta}{2\pi}\frac{d\phi}{2\pi}\int d^3v\frac{\vec{v}\times\vec{n}\cdot\nabla\psi}{\Omega|\nabla\psi|}\left[C(f_0,\tilde{f}_1) + C(\tilde{f}_1,f_0)\right] = 0 \qquad (42)
\end{aligned}
$$

where the symmetric part of the drift velocity is

$$
\vec{v}_{dz}^{\,s} = \frac{1}{\Omega}\vec{n}\times(\mu\nabla\vec{B} + v_\parallel^2\vec{n}\cdot\nabla\vec{n}) \ , \qquad (43)
$$

and the drift velocity due to ripple is

$$
\vec{v}_{dz}^{\,r} = \frac{1}{\Omega}\vec{n}\times(-\mu B_0\nabla\delta + v_\parallel^2\vec{n}\cdot\nabla\vec{n}_\delta) \ . \qquad (44)
$$

Then the inflow flux is

$$
\Gamma_{in} = \int\frac{d\theta}{2\pi}\frac{d\phi}{2\pi}\int\frac{2\pi B d\mu d\varepsilon}{|v_\parallel|}\left[\vec{v}_{dz}^{\,s}\cdot\frac{\nabla\psi}{|\nabla\psi|}\overline{f}_1 + \vec{v}_{dz}^{\,r}\cdot\frac{\nabla\psi}{|\nabla\psi|}f_0\right] \ . \qquad (45)
$$

The second term can be called a kinematic flow term. The first term is the ripple diffusion term for trapped particles and can be interpreted as a parallel friction term for circulating particles. A detailed solution of the kinetic equation, taking into account the

gradient of the ripple field, the increase of the length of the field line, and the change of q value has to be carried out in order to evaluate the first term; this is the topic of the continuing study. A brief discussion of the physical nature of the parallel friction and its effect will be given later. The estimate of the inflow flux coming from the second term is discussed below.

$$\Gamma_{in} = \int \frac{d\theta}{2\pi}\frac{d\phi}{2\pi}\int \frac{2\pi B d\mu d\varepsilon}{|v_\parallel|}\frac{1}{2\Omega}\left(2v_\parallel^2 + v_\perp^2\right)\sin\theta\frac{d\delta}{dR}$$

$$\cdot n\left(\frac{M}{2\pi T}\right)^{3/2}\exp\left(-M\varepsilon/T\right)$$

$$= \frac{\pi\sqrt{2}}{\Omega}n\left(\frac{M}{2\pi T}\right)^{3/2}\int \frac{d\theta}{2\pi}\frac{d\phi}{2\pi}\int B d\mu d\varepsilon \frac{(2\varepsilon - \mu B)}{\sqrt{(\varepsilon - \mu B)}}\exp\left(-M\varepsilon/T\right)\sin\theta\frac{d\delta}{dR}\ . \qquad (46)$$

For circulating particles we have to consider the integrand

$$I = \int_0^{\mu_T} d\mu \frac{2\varepsilon - \mu B}{\sqrt{\varepsilon - \mu B}}\ , \qquad (47)$$

where $\mu_T = \varepsilon/(1+\epsilon)B_0$ is the boundary for the barely circulating and trapped particles. Expanding the denominator in $\mu B/\varepsilon$ and keeping the first order we have

$$I = \int_0^{\mu_T} 2\varepsilon^{1/2}\left[1 - \left(\frac{\mu B}{2\varepsilon}\right)^2\right]d\mu \simeq \frac{2\varepsilon^{3/2}}{B_0}(1-\epsilon)\ . \qquad (48)$$

We easily obtain the integrand

$$\int_0^\infty \varepsilon^{3/2}\exp(-M\varepsilon/T)d\varepsilon = \frac{3}{4}\sqrt{\pi}\left(\frac{T}{M}\right)^{5/2}\ . \qquad (49)$$

Therefore the inflow flux becomes

$$\Gamma_{in} \simeq \frac{3nT(1-\epsilon)}{4\Omega M}\frac{1}{(2\pi)^2}\int\int \frac{B}{B_0}\sin\theta\frac{\partial\delta}{\partial R}d\theta d\phi\ . \qquad (50)$$

From Eq. (4)

$$\frac{\partial\delta}{\partial R} = \frac{\delta_0}{a}\left\{\left[\frac{1}{2} + c\left(\frac{r\cos\theta + a}{2a}\right) + \frac{k\cos\theta}{r}\left[\frac{r\cos\theta + a}{2a} + c\left(\frac{r\cos\theta + a}{2a}\right)^2\right]\right]\cos^m\frac{\theta - \theta_0}{2}\right.$$

$$+\left[\frac{r\cos\theta+a}{2a}+c\left(\frac{r\cos\theta+a}{2a}\right)^2\right]\frac{m}{2}\frac{a}{r}\sin\theta\sin\frac{\theta-\theta_0}{2}\cos^{m-1}\frac{\theta-\theta_0}{2}\Bigg\}$$

$$\left(\frac{r}{a}\right)^k\cos\left(\frac{\phi}{\lambda}\right)\exp\left[-\left(\frac{\phi}{\alpha}\right)^2\right]. \tag{51}$$

The integration over θ in Eq. (50) is approximated by $\left(\frac{\partial}{\partial R}\delta\,|_{\theta=\theta_0}\right)\cdot\Delta\theta$ where $\Delta\theta=\pi/2$ is the half width. We are left to consider the integration

$$\int_{-\pi}^{\pi}\cos\left(\frac{\phi}{\lambda}\right)\left[-\left(-\frac{\phi}{\alpha}\right)^2\right]d\phi\,. \tag{52}$$

The integrand is approaching zero quickly outside the ripple. The integration can be approximated by the difference of functional values of the integrand at $\phi=0$ and ϕ_1 multiplied by $2\phi_1=2\pi/N$, the width of the ripple from peak to peak. The inflow flux now becomes

$$\Gamma_{in}\simeq\frac{-3}{32}\frac{nT\delta_0(1+c)}{\Omega MaN}(1-\epsilon)\left(\frac{r}{a}\right)^k\left[1-\cos\left(\frac{\phi_1}{\lambda}\right)e^{-(\phi_1/\alpha)^2}\right]. \tag{53}$$

Plugging in the constants for the ripple, this equation becomes

$$\Gamma_{in}\approx-1.56\times10^{-3}\frac{nT}{\Omega Ma}(1-\epsilon)\left(\frac{r}{a}\right)^2. \tag{54}$$

This inward flow is proportional to the temperature T, $(1-\epsilon)$, and the ripple amplitude, and is inversely proportional to the magnetic field B_0 and charge q_j through Ω and the minor radius a. If the temperature is flat, the dependence of the flow on r is exponential. For high Z impurities which are normally in high charge state, the influx is reduced by a factor of Z_I. For the same reason, the inflow of helium ions is also a factor of 2 smaller than that of fuel ions.

The contributions from the increase of length and change of q value have been discussed in Section 3.2. There is possibly a contribution to the flux arising from the parallel flow caused by the radial displacement of the counter-streaming particles. The physics bears a resemblance to the mechanisms operating in producing the ionic bootstrap current as discussed by Molvig [32,33]. Assuming that the radial profile of the counter-streaming particles maintain its central peak, the inward flux of this species will produce a local

deficit of counter-streaming particles, or, in other words, a co-streaming flow. This flow in turn produces a collisional drag on the remaining population in a direction parallel to both the equilibrium electric current and the ohmic force on the ions. Thus, just as the electric field causes the Ware pinch, so this calculation given above for the inward flow is, at worst, a lower bound. The radial electric field may also contribute. Qualitatively the co-streaming flow will produce $E_r > 0$ which is known to drive impurities outward [34].

Using the reactor parameters given in Section 2.0, at $r = 120$ cm and $T_i = 10$ keV, the influx is approximately $\Gamma_{in} = -72.9$ n. The inflow velocity is

$$v_{in} = -72.9 \text{ cm/sec} . \tag{55}$$

The inflow velocity is calculated by using the Monte Carlo method on test particles which gives -39.5 cm/sec. The test particles, isotropical in phase space and with Maxwellian energy distribution, were launched on midplane at $r = 120$ cm and $\phi = 180°$. The integration over energy was carried out by using Gaussian quadrature techniques where ten energy intervals were used. The collision of the test particles with the background plasma was included. The agreement in velocity indicates that the theoretical estimate is reasonable. The significance of this inflow velocity can be seen by making a comparison with the outflow due to neoclassical diffusion and anomalous diffusion. The peak density for the model reactor considered is $n_0 = 3 \times 10^{14}$ cm^{-3}. Assuming a parabolic density profile, the correspondence density at $r = 120$ cm is $n = 1.3 \times 10^{14}$ cm^{-3} and for $T_e = 10$ keV, the collision frequency is

$$\begin{aligned} \nu_{ei} &= \frac{4\sqrt{2\pi} n_i Z^2 e^4 \ln\Lambda}{3\sqrt{m_e} T_e^{3/2}} \\ &= 1.5 \times 10^4 \left(\frac{n_e}{10^{13}\text{cm}^{-3}}\right) \Big/ \left(\frac{T_e}{1\text{keV}}\right)^{3/2} \text{sec}^{-1} \end{aligned} \tag{56}$$

which gives us 6.2×10^3 sec^{-1}. The ratio of the collision frequency with $\omega_t = v_{th}/qR$, the transition frequency, is

$$\frac{\nu_{ei}}{\omega_t} = 9.70 \times 10^{-4} \tag{57}$$

which is less than $\epsilon^{3/2} = (r/R)^{3/2} = 7.75 \times 10^{-2}$. Therefore it is in the banana regime and the diffusion coefficient is [35]

$$D_b = \nu \rho^2 q^2 \epsilon^{-3/2} = 4.97 \text{ cm}^2/\text{s} . \tag{58}$$

Then outflow velocity is

$$V_{out}^D = D_b \frac{2r/a^2}{1-(r/a)^2} = 10.66 \text{ cm/s} . \tag{59}$$

For the anomalous outflow we use the three particle transport models used in references [1,36-38]

$$\text{(1)} \qquad D_p = \frac{10^{17}}{n_e \text{ (cm}^{-3})} \text{ cm}^2/\text{s} = 7.62 \times 10^2 \text{ cm}^2/\text{s} ,$$

$$V_p = 16.33 \text{ cm/s} , \tag{60}$$

$$\text{(2)} \qquad D_p = \frac{2.5 \times 10^{19}}{q n_e \text{ (cm}^{-3})[T_e(\text{eV})]^{3/4}} \text{ cm}^2/\text{s} = 1.36 \times 10^2 \text{ cm}^2/\text{s} ,$$

$$V_p = 2.92 \text{ cm/s} , \tag{61}$$

$$\text{(3)} \qquad D_p = 10^3 \times [1 + 9(r/a)^2] \text{ cm}^2/\text{s} = 6.06 \times 10^3 \text{ cm}^2/\text{s} ,$$

$$V_p = 129.93 \text{ cm/s} . \tag{62}$$

Therefore, kinematic inflow velocity is greater than the outward flow velocity due to neoclassical diffusion given by Eq. (59) and models 1 and 2 anomalous diffusion given by Eqs. (60) and (61) and less than the velocity due to the anomalous diffusion given by Eq. (62). However, they are all within comparable magnitude; thus, the kinematic inflow induced by the asymmetric ripple can make a significant contribution to particle control.

5.0 Beam Injection

By examining the particle orbit drifts discussed in earlier sections, it is seen that the penetration of an injected beam can be enhanced in two ways. One way is to inject the beam into the ripple perpendicularly as proposed by Jassby and Goldston [29]. The other way is to inject the beam into the axisymmetric region tangentially in the counter-streaming direction. In the first injection scheme, the drift penetration is largest when $\chi \simeq 0$. Direct injection into the valley at 90° is difficult with the specific coil configuration. However, the penetration depth is not a sharp function of χ which permits slight deviation from the 90° injection.

In the second scheme the penetration speed has been calculated as a function of χ for energy from 10 keV to 100 keV in steps of 10 keV and is presented in Fig. 21. The top curve (dashed line labelled by open triangle) is for 10 keV beam energy. The bottom curve (solid line labelled by open square) is for 100 keV beam energy. Generally, the penetration speed increases with both χ and beam energy. The variation of speed with both χ and energy is not steep; therefore, the injection angle and the beam divergence are not critical. The variation of penetration speed with respect to χ shows large fluctuation below 70 keV and becomes much smoother for energy greater than 80 keV. an energy of 80 keV can then be considered the lower limit. Therefore, the energy requirement is much lower than that predicted or the perpendicular injection [29]. A 100 keV particle could reach the center in about 300 ms.

6.0 Concluding Discussion

It was shown in the above discussion that an convective influx can be induced by using a specially structured vertical asymmetric ripple. The major contribution to the influx is from the counter-streaming circulating particles. The key features of the ripple are that the well depth is much larger than the peak amplitude and that the averaged gradient of the toroidal field was increased on the drifting surfaces below midplane. This increased gradient enhances the inward drift of circulating particles and of about half the banana

particles which are not compensated in the axisymmetric region outside the ripple and above midplane. It appears that there is very little adverse effect on the confinement of banana particles.

The inflow flux was found to be proportional to $(1-\epsilon)$, density n, the ripple amplitude δ_0. It is inversely proportional to the charge q_j, toroidal magnetic field B_0 and minor radius a. If the temperature is flat the dependence of the inflow on (r/a) is exponential. The inflow for high Z impurity species is a factor of Z_I less than that of fuel ions. The inflow velocity is about the order of the outflow velocity due to anomalous diffusion. The effect of multiple ripple, ripple amplitude and width have to be evaluated. The same concept can also be applied to the neutral beam injection. The enhancement of neutral beam penetration can be achieved by injecting the beam at the outboard plasma edge on the midplane as well as into the ripple perpendicularly. The influx can probably be further enhanced by heating the ions using rf power.

The coil configuration used in this study was for the convenience of numerical computation and can be further optimized. Engineering considerations are always kept in mind. The distance between the plasma and the center of the coil conductor is 70 cm so that adequate shielding can be provided to protect the coil. The total width of the coil set is slightly smaller than the gap between the TF coils so that it can be inserted and removed easily. The 1 MA coil current does not present any engineering problems.

The scraping off occurs when the large banana particles intersect the wall in one orbit [25,39]. It takes several orbits for the tip of a banana particle to drift into and be affected by the ripple field. The scraping off of the energetic banana alpha particles is not affected by the ripple and will leave the plasma as usual. Therefore, ash removal is not affected. The heavy metal impurity level is reduced due to the reduction of wall bombardment by ions. However, careful investigation in these areas is required.

Acknowledgment

The author is grateful to K. Molvig and J. Johnson for their comments. This work was supported by the US Department of Energy under Contract No. DE-AC02-78ET51013.

Figure Captions

Fig. 1. Magnetic field magnitude along minor radius on midplane for a prototypical tokamak reactor with 12 TF coils. The dashed curve is the axisymmetric field. The solid curve above the dashed curve is the field at 15° and the solid curve below the dashed curve is the field at 0°.

Fig. 2. Ripple coil configuration; (a) perspective view; (b) cross sectional view; (c) top view.

Fig. 3. The shape of ripple at the bottom of the plasma surface and the vertical variation. The ripple magnitude decreases toward the midplane. The insert on the upper right hand corner shows the magnified ripple on the bottom line.

Fig. 4. The vacuum toroidal field along the perimeter of lower half of the plasma surface; the variation of the field along the major radius for an axisymmetric tokamak (solid curve), the variation of the field along the major radius in the valley of the ripple well (dashed curve) and on the peak of the ripple (dotted curve).

Fig. 5. Perspective view of the ripple on the lower half of the plasma surface. The ripple forms a trough on the surface below the midplane.

Fig. 6. The contour of the ripple over the plasma cross section. The ripple increases toward the boundary and diminishes above the midplane.

Fig. 7. The variation of the toroidal magnetic field with ripple along a field line passing through the lowest point of the plasma.

Fig. 8. The orbit of a particle launched in the ripple well. $E = 10$ keV, $R = 500$ cm, $\phi = 0°$, $Z = 195$ cm, $\chi = 0.1$.

Fig. 9. The penetration depth as a function of χ for 10 keV particle trapped in the ripple.

Fig. 10. The orbit of a counter-streaming circulating particle ($\chi = 0.8$) with $E = 3.5$ MeV, $R = 680$ cm, $\phi = 180°$, and $Z = 0.0$. The counter-streaming particle is spiraling toward the center from the initial point 0.

Fig. 11. The orbit of a co-streaming circulating particle ($\chi = -0.8$) launched at the same position at in Fig. 10. It shows very small deviation from the drift orbit in an axisymmetric field.

Fig. 12. The field variation as a function of time along the orbit of a counter-streaming and co-streaming circulating particle (dashed curves).

Fig. 13. Deeply trapped banana particles which drift out due to tip scattering on the peak of the ripple. Particle was launched at point 0 ($R = 660$ cm, $\phi = 180°$, $Z = 0$, $\chi = 0.20$).

Fig. 14. The banana orbit was driven inward at the lower tip by the gradient of the ripple. It was launched at point 0 ($R = 660$ cm, $\phi = 147°$, $Z = 0$, $\chi = +0.5$) and drifted through point f.

Fig. 15. Banana particle launched at $R = 660$ cm, $\phi = 180°$, $Z = 0$, $\chi = +0.5$ which drifts inward due to multiple passes through the ripple well and becomes a circulating particle.

Fig. 16. Banana particle $\chi = -0.5$ launched at the same position given in Fig. 15. It also drifts inward and becomes circulating.

Fig. 17. Drift boundary in the phase space. The shaded regions ($-0.22 < \chi < 0.22, 0.32 < \chi < 0.47$) are outward-drifting banana particles. The region $-0.47 < \chi < 0.22$ and $0.22 < \chi < 0.32$ are inward drifting banana particles. The counter-streaming circulating particles are drifting inward.

Fig. 18. The drifting velocity as a function of χ. The net drifting of banana particles is nearly zero. Counter-streaming particles drift inward at high speed. The majority of the co-streaming particles drift inward, but at a lower speed.

Fig. 19. The orbit of a 10 keV particle launched in the ripple ($\chi = -0.3$, $R = 500$ cm, $\phi - 0$, $Z = -195$ cm). It quickly becomes a banana orbit as shown by the heavy line, and then becomes a circulating orbit as shown by the light lines due to collision and ripple.

Fig. 20. The collision effect on the particle orbit. The variation of χ as a function of time which shows χ approaching 0.6 after many collisions and much drifting.

Fig. 21. Penetration speed as a function of χ for a beam injected at the plasma edge for energy from 10 keV (top dashed curve labelled with open triangle) to 100 keV (bottom solid curve labelled with open square) in 10 keV steps. The curves for the other energies are given by the legend on the lower left corner.

References

[1] Coppi, B., Sharky, N., Nucl. Fusion 21 (1981) 1363.

[2] Dnestrovkij, Yu. N., Neudatchin, S. V. and Pereverzev, G. V., Sov. J. Plasma Phys. 10 (2) (1984) 137.

[3] Dnestrovkij, Yu. N., Lysenko, S. E., Neudatchin, S. V. et al., 10th Eur. Conf. on Contr. Fus. and Plasma Phys., Vol. I, Moscow (1981) B-15.

[4] Strachan, J. D., Bretz, N., Mazzucato, E., et al., Nucl. Fusion 22 (1982) 1145.

[5] Marmar, E. S., J. of Nucl. M. 76/77 (1978) 49.

[6] McCracken, G. M., Stott, P. E., Nucl. Fusion 19 (1979) 889.

[7] Seki, Y., Shimamura, Y., Marki, K., Nucl. Fusion 20 (1980) 1213.

[8] Heifetz, D., Post, D., Petravic, M., Wesiheit, J., PPPL-1843 (Nov. 1981).

[9] Post, D. E., Heifetz, J., Petravic, M., PPPL-1913 (July 1982).

[10] INTOR, European Contributions- Phase IIA, Vol. II, Brussels (August 1985).

[11] INTOR, European Contributions- Phase IIA, Vol. I, (19 USA INTOR/85-1).

[12] Anderson, O. A., Furth, H. P., Nucl. Fusion 12 (1972) 207.

[13] Goldston, R. J., White, R. B., Boozer, A. H., Phys. Rev. Lett. 47 (1981) 647.

[14] Frieman, E. A., Phys. Fluids 13 (1970) 490.

[15] Stringer, T. E., Nucl. Fusion 12 (1972) 689.

[16] Connor, J. W., Hastie, R. J., Nucl. Fusion 13 (1973) 221.

[17] Krommes, J. A., Rutherford, P. M., Nucl. Fusion 14 (1974) 695.

[18] Yang, T. F., Emmert, G. A., in Tech. of Contr. Nucl. Fusion (Proc. 1st Top. Meeting) USAEC-CONF-740402-P2 (1974).

[19] Davidson, R. C., Neal, J., Nucl. Fusion 16 (1976) 731.

[20] Tsang, K. T., Nucl. Fusion 17 (1977) 557.

[21] Goldston, R. J., and Towner, H. H., Princeton Plasma Physics Laboratory Report No. PPPL-1637, 1980 (unpublished).

[22] Boozer, A. H., Phys. Fluids 23 (1980) 2283.

[23] Shaing, K. C., Callen, J. D., Phys. Fluids 25 (6) (1982) 1012.

[24] Yushmanov, P. N., Nucl. Fusion 22 (1982) 1199, and Nucl. Fusion 22 (1982) 315.

[25] McAlees, D. G., Alpha Particle Energetics and Neutral Beam Heating in Tokamak Plasmas, Rep. ORNL-TM-4661, Oak Ridge National Laboratory, TN (1974).

[26] Mynick, H. E., Nucl. Fusion 26 (1986) 491.

[27] Mudford, B. S., Johnson, P. C., Plasma Phys. and Contr. Nucl. Fusion 27 (1985) 1461.

[28] Potok, R. E., Politzer, P. A., Lidsky, L. M., Phys. Rev. Lett. 45 (1980) 1328.

[29] Jassby, D. L., Goldston, R. J., Nucl. Fusion 104 (1976) 613.

[30] INTOR, US contributions (1979)

[31] Stott, P. E., Wilson, C. M., Gibson, A., Nucl. Fusion 17 (1977) 481.

[32] Molvig, K., Hizanidis, K., Phys. Fluids 27 (12) (1984) 2847.

[33] Molvig, K., Lidsky, L. M., Hizanidis, K., and Bernstein, I. B., Comments of Plasma Phys. and Contr Fus. 7 (4) (1982) 113.

[34] Sigmar, D. J., "Alpha Particle Effects in Burning Tokamak Plasma; Overview and Specific Examples", MIT Plasma Fusion Center Report PFC/CP-86-9 (1986) and all references cited.

[35] Hinton, F. L. Hazeltine, R. D., Rev. Mod. Phys. 48 Part I (1976) 239.

[36] Post, D. E., Goldston, R. J., Grimm, R. C., Hawryluk, R. J., Hirshman, S. P., Hsieh, D., Hulse, R. A., Jassby, D. L., Jensen, R. V., McKenney, A., Meade, D. M., Kikkelsen, D. R., Odgen, J. M., Okabayashi, M., Rutherford, P. H., Schmidt, J. A., Seidl, F. G. P., Suckewer, S., Tenney, F., Mirin, A. A., McCoy, M. G., Killeen, J., Rensink M. E., Shumaker, D. E., Tarter, C. B., in Plasma Phys. and Contr. Nucl. Fusion Res. (Proc. 7th Int. Conf., Innsbruck, 1978) Vol. 1, IAEA, Vienna (1979) 471.

[37] Stambaugh, R. D., Rawls, J. M., Nucl. Fusion 19 (1979) 983.

[38] Mercier, C., Werkoff, F., Morera, J. P., Cissoko, G., Capes, H., Nucl. Fusion 21 (1981) 291.

[39] Tani, K., Takizuka, T., Azumi, M., Kishimoto, H., Nucl. Fusion 23 (1983) 657.

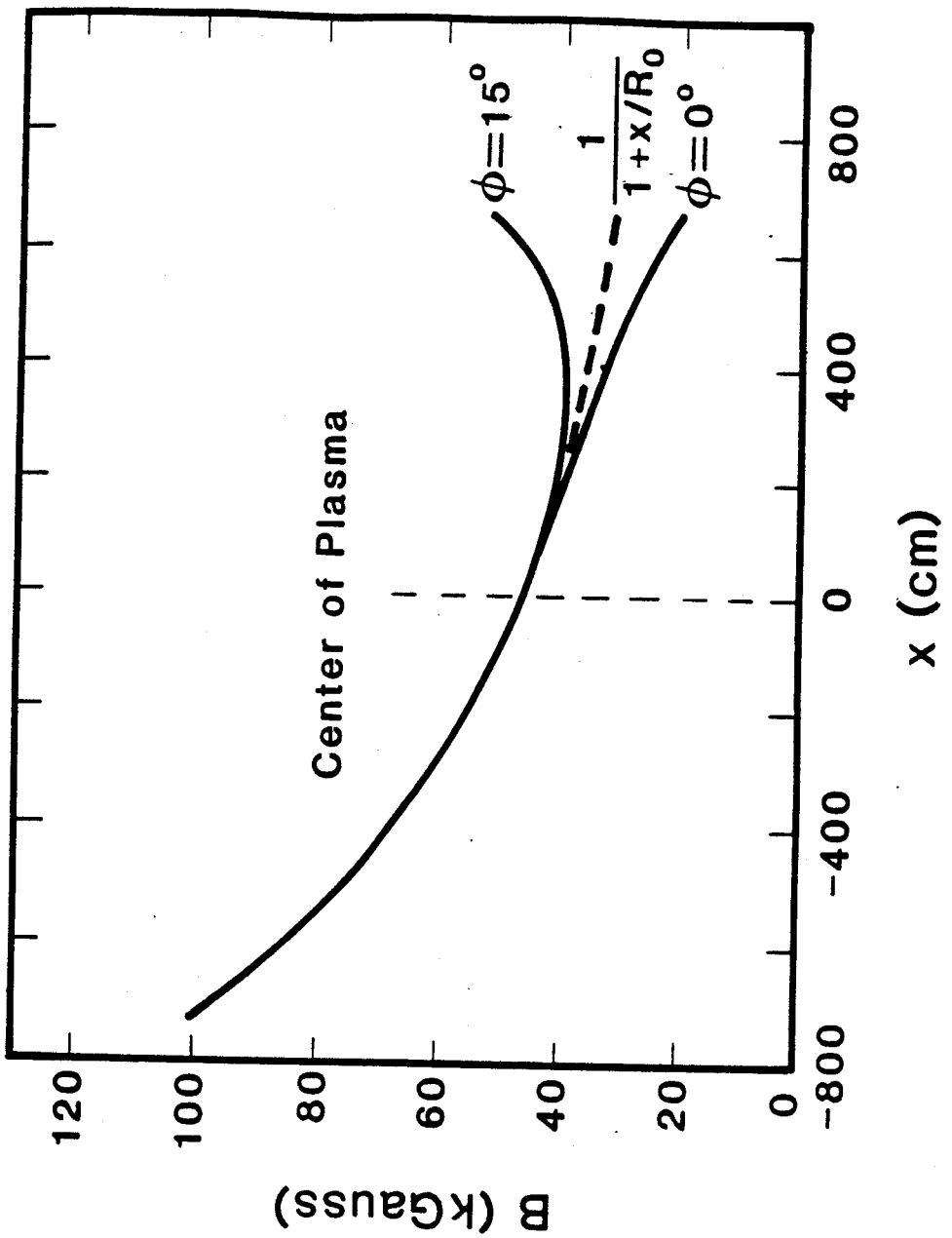
B (kGauss)
120
100
80
60
40
20
0
-800
-400
0
400
800
x (cm)
Center of Plasma
ϕ=15°
$\frac{1}{1+x/R_0}$
ϕ=0°

Figure 1

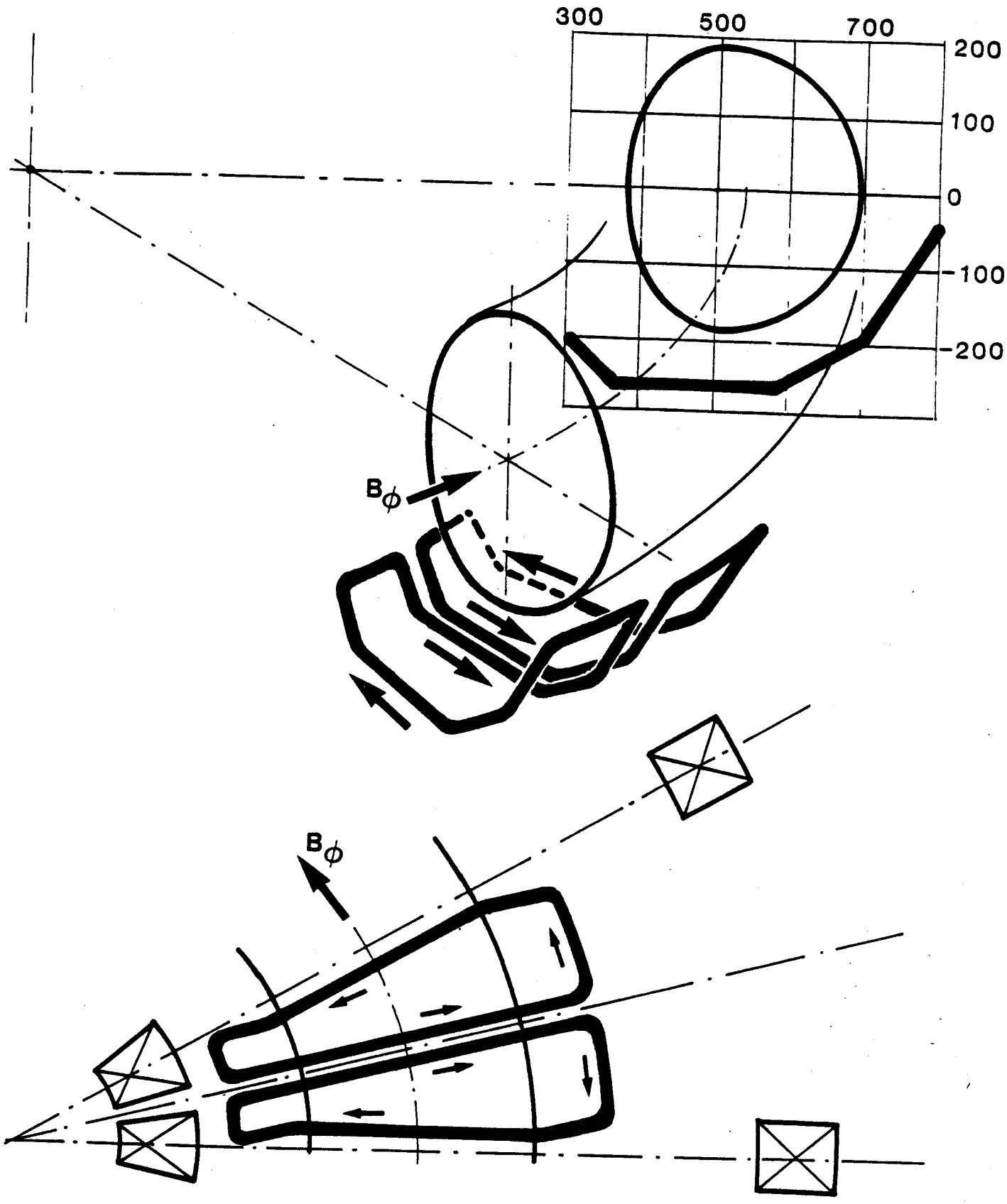

Figure 2

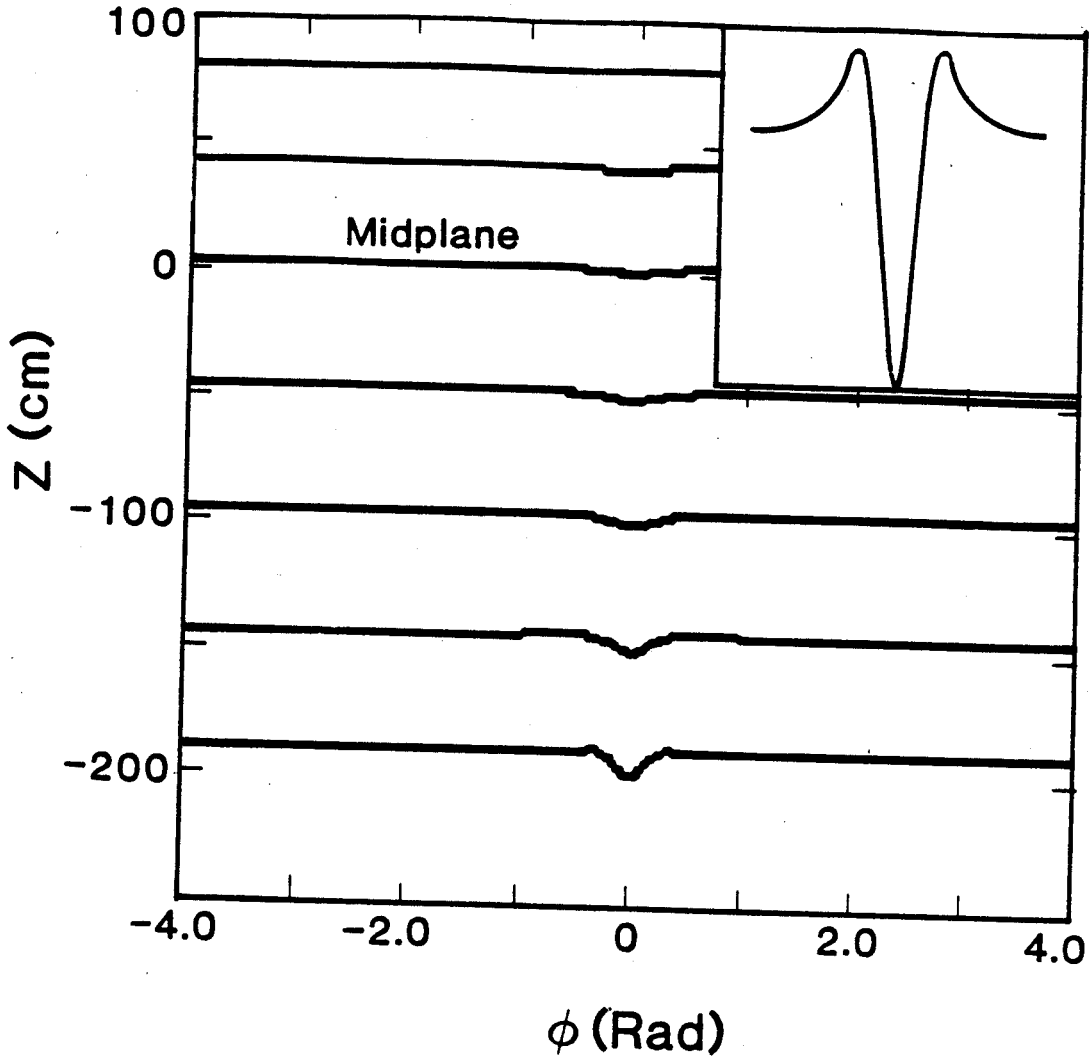

Figure 3

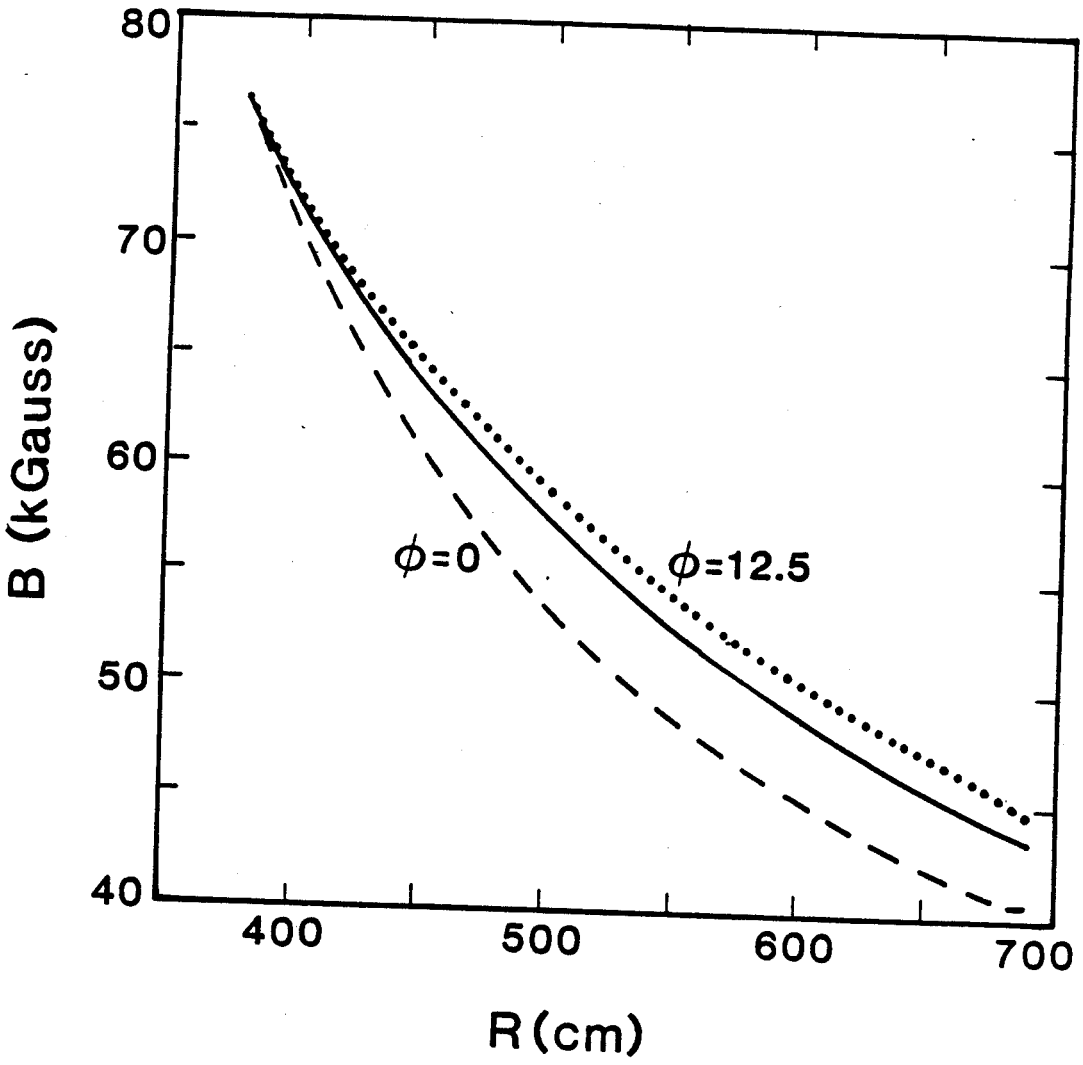

Figure 4

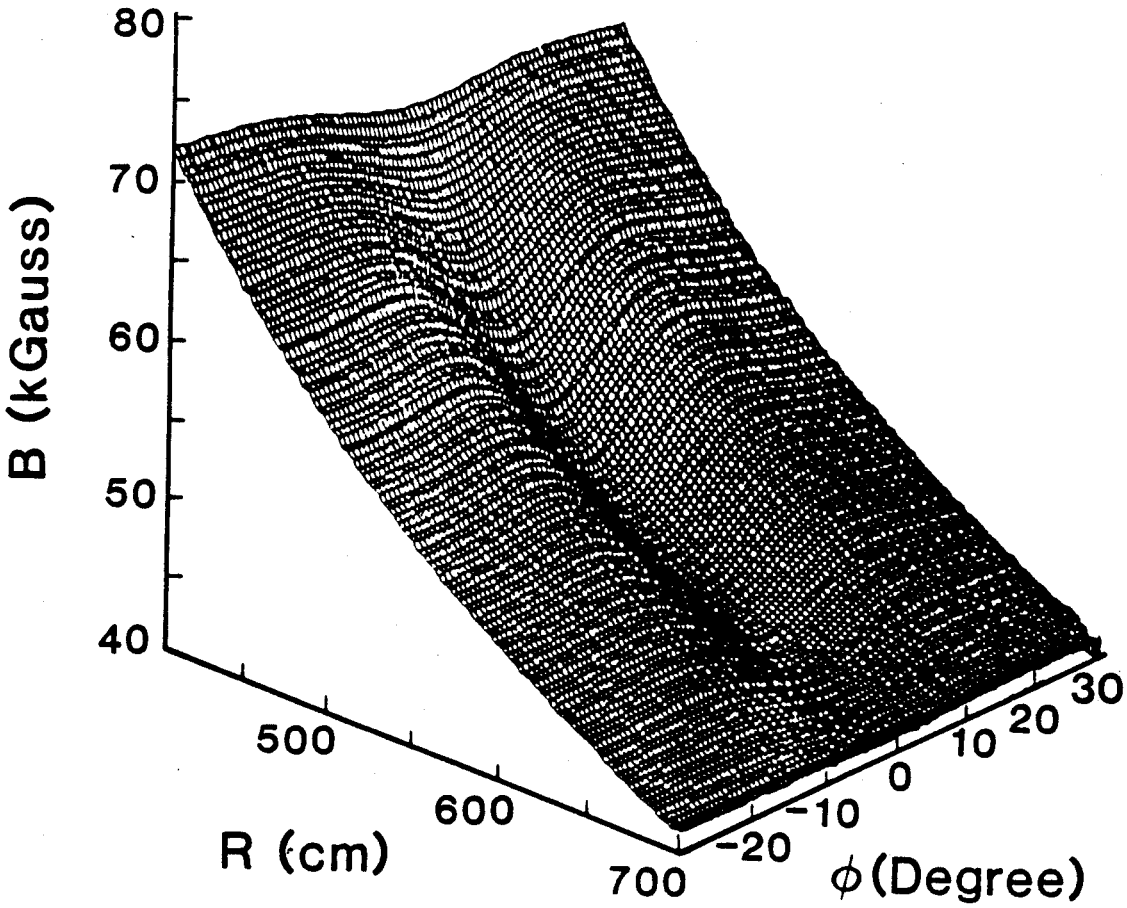

Figure 5

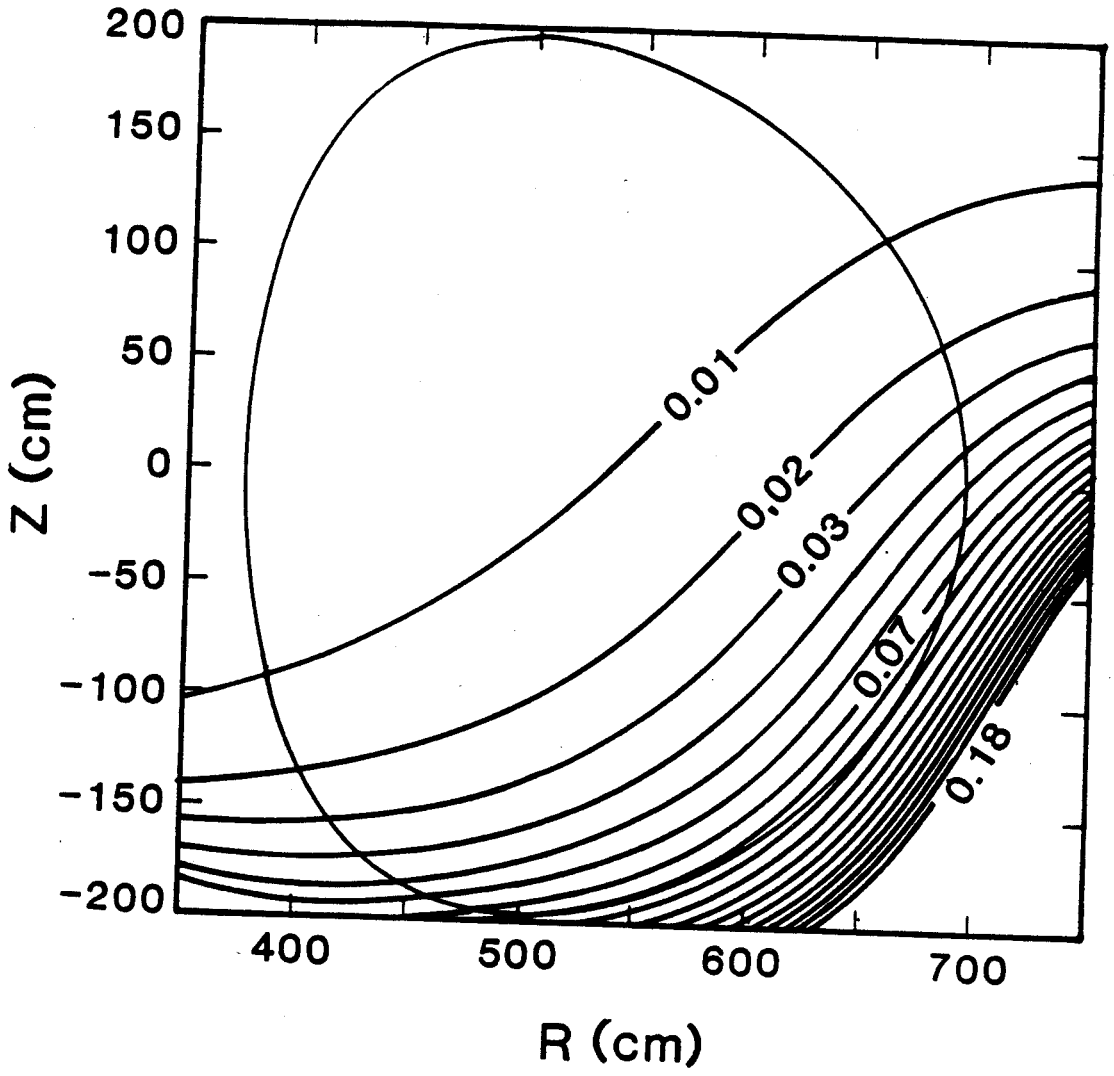
200
150
100
50
0
-50
-100
-150
-200
Z (cm)
400
500
600
700
R (cm)
0.01
0.02
0.03
0.07
0.18

Figure 6

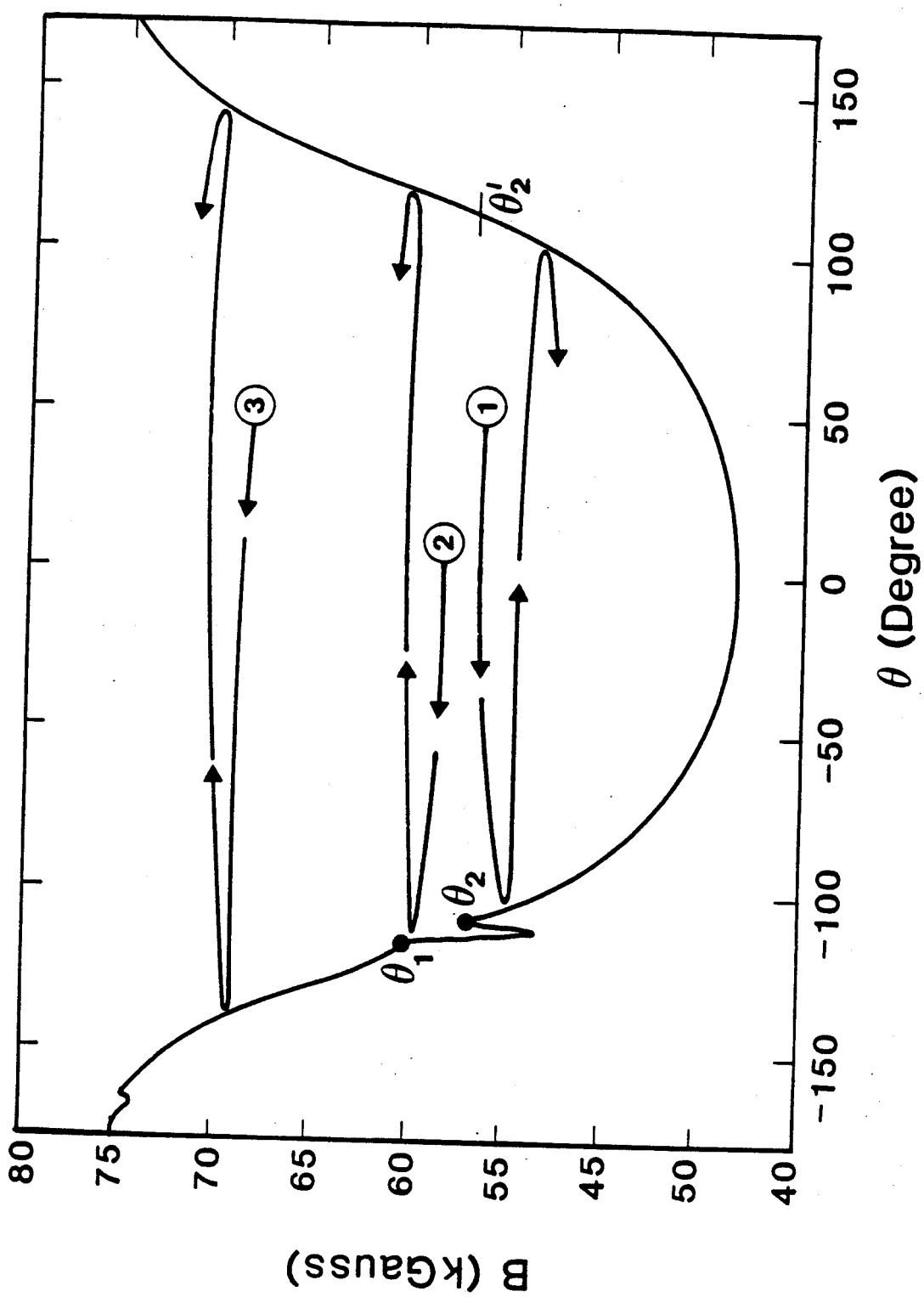
B (kGauss)
80
75
70
65
60
55
45
50
40
θ (Degree)
150
100
50
0
-50
-100
-150
θ'2
θ2
θ1
1
2
3

Figure 7

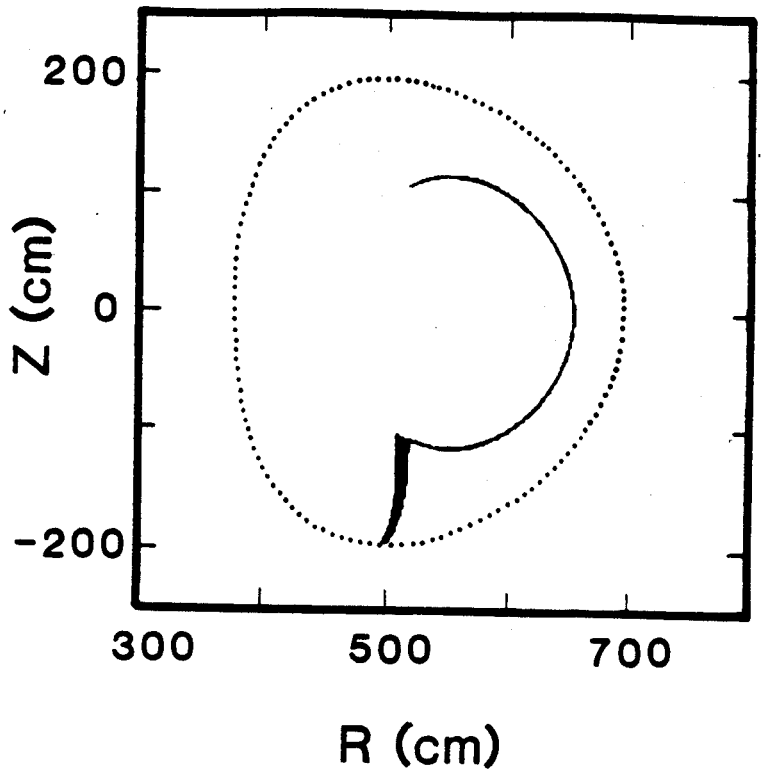

Figure 8

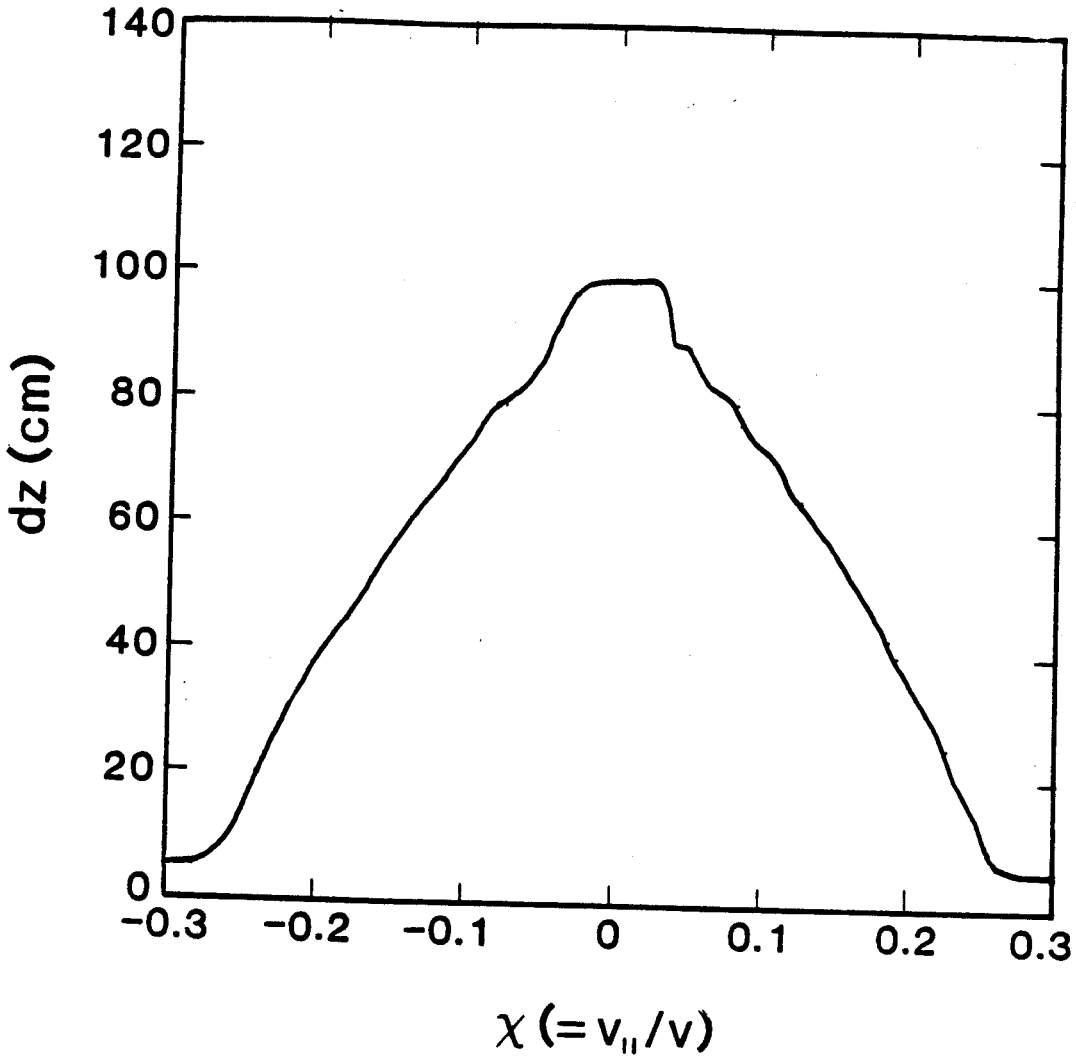

Figure 9

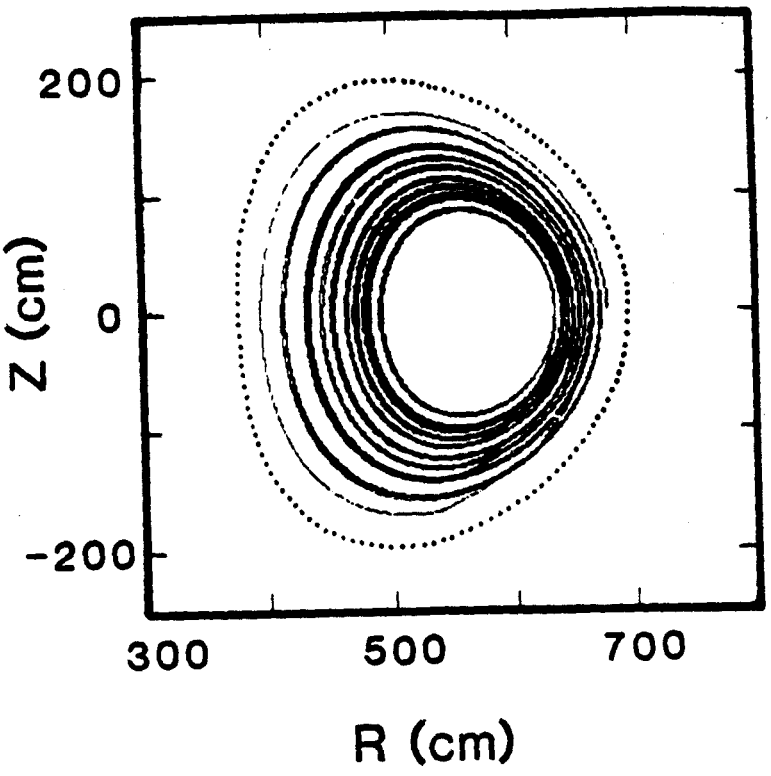

Figure 10

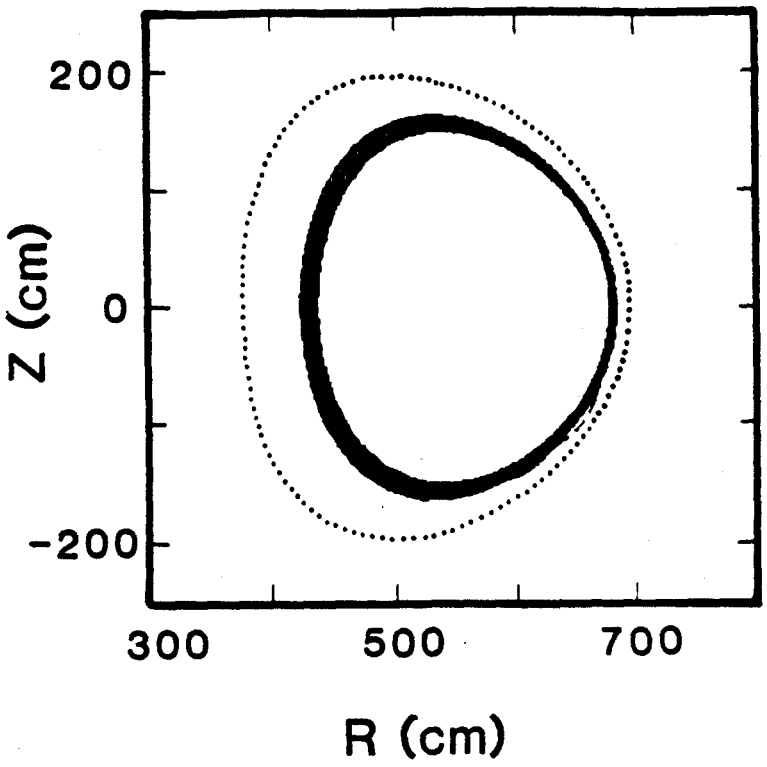

Figure 11

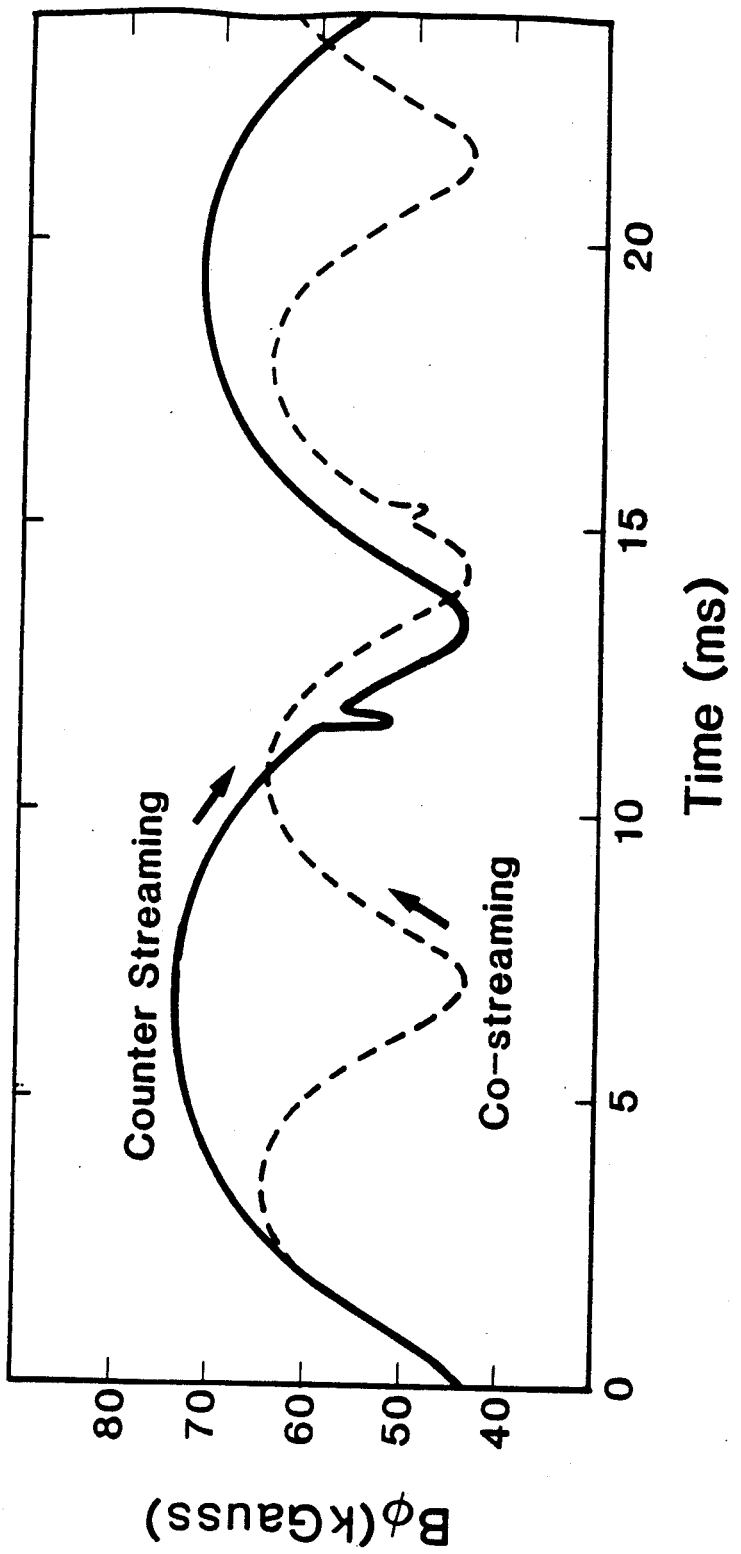
Bφ(kGauss)
80
70
60
50
40
0
5
10
15
20
Time (ms)
Counter Streaming
Co-streaming

Figure 12

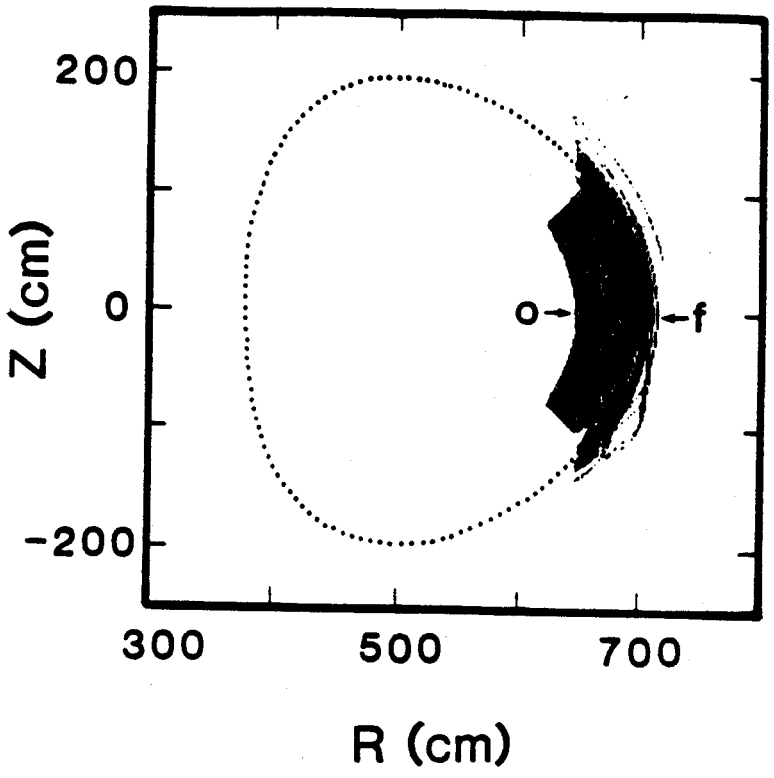

Figure 13

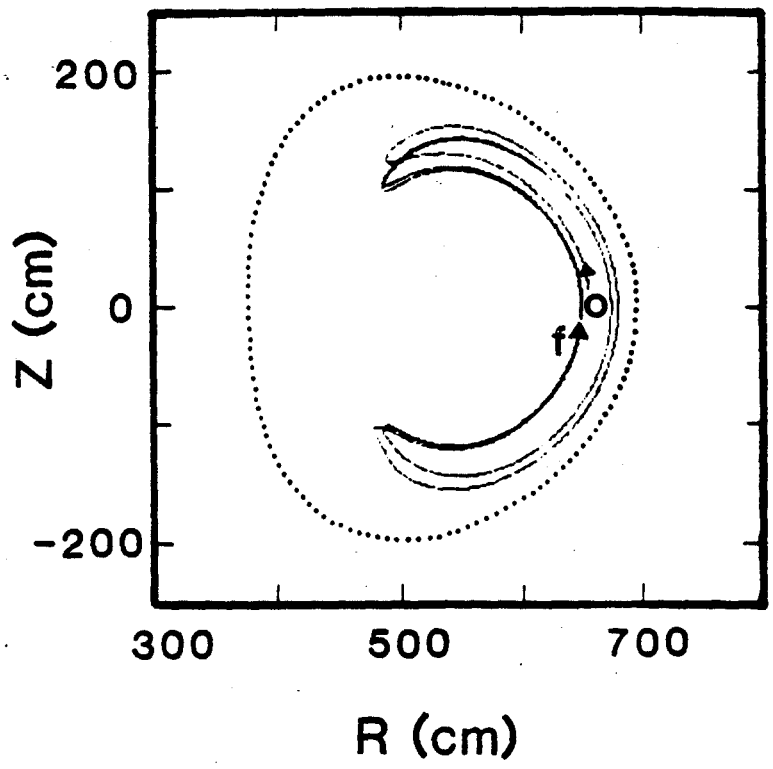

Figure 14

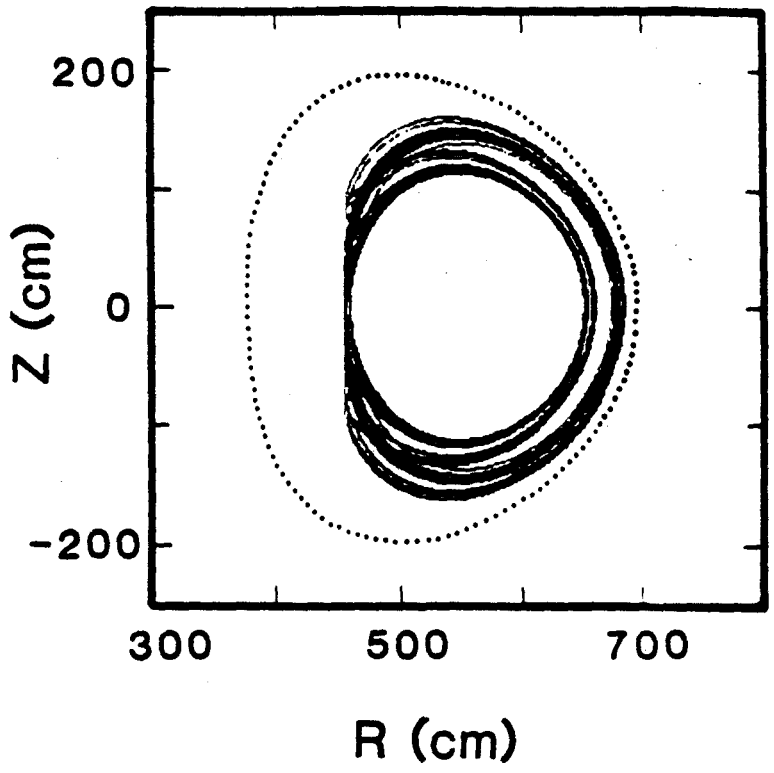

Figure 15

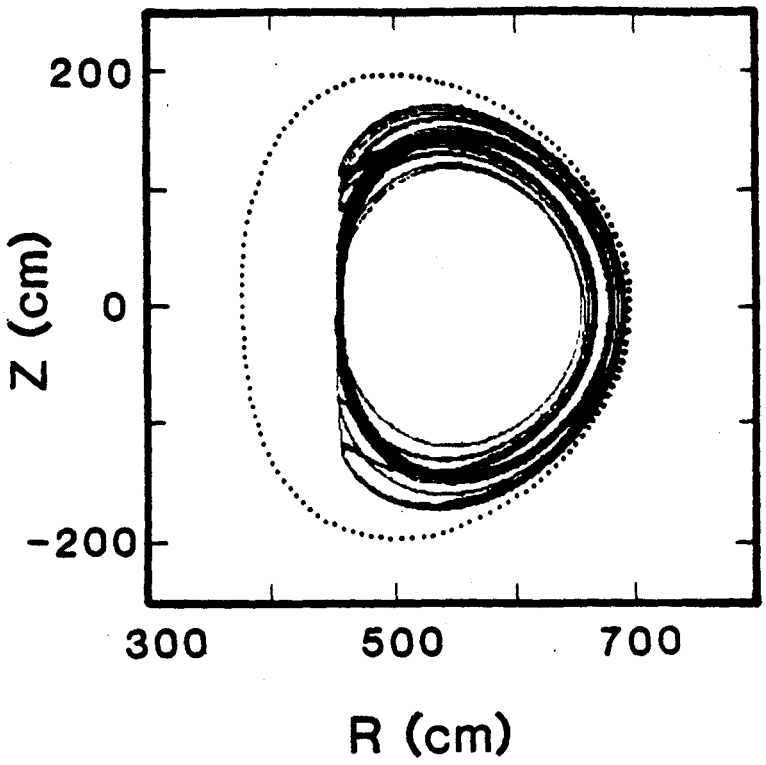

Figure 16

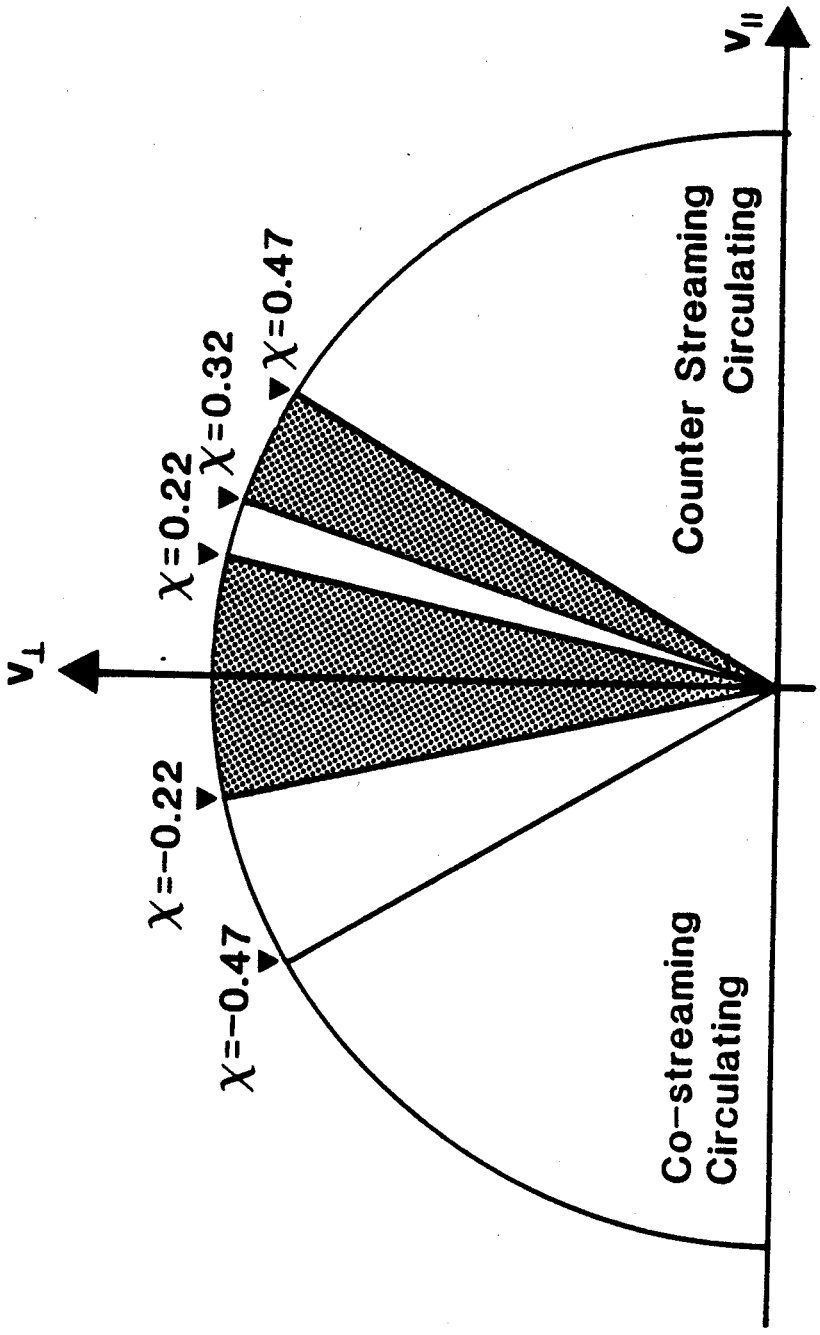
$v_{\parallel}$
$v_{\perp}$
Counter Streaming
Circulating
Co-streaming
Circulating
χ=0.47
χ=0.32
χ=0.22
χ=−0.22
χ=−0.47

Figure 17

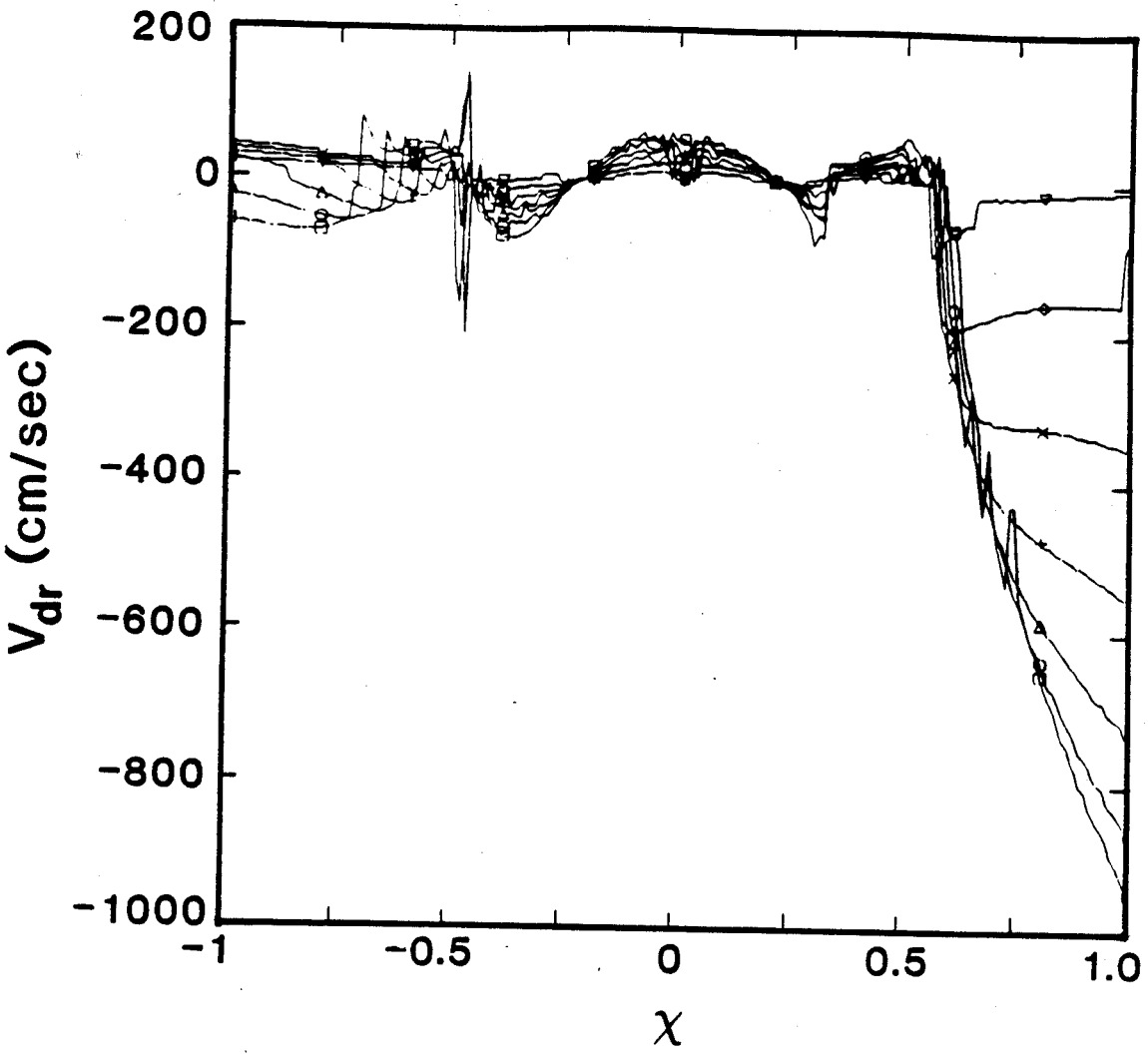

Figure 18

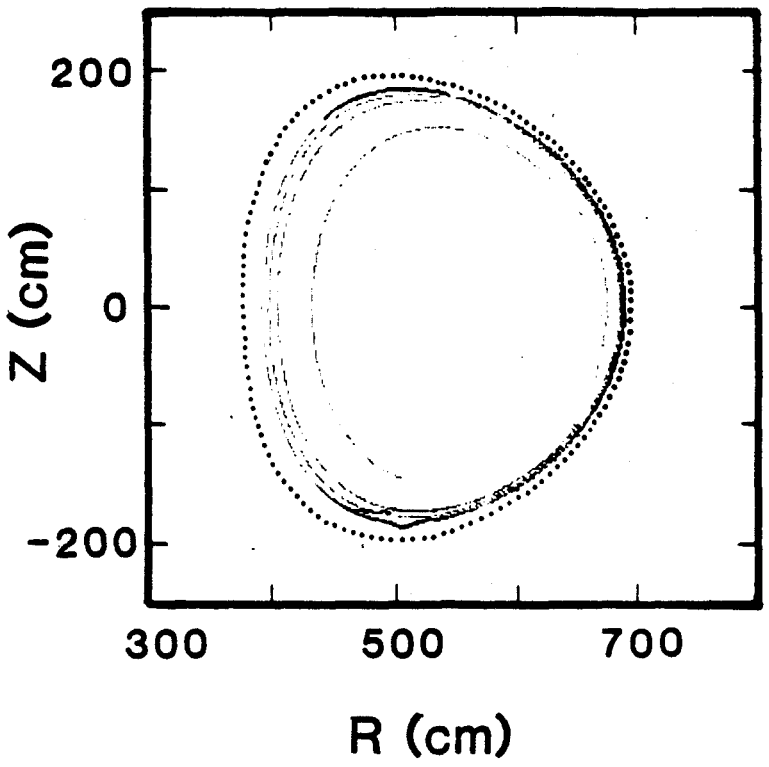

Figure 19

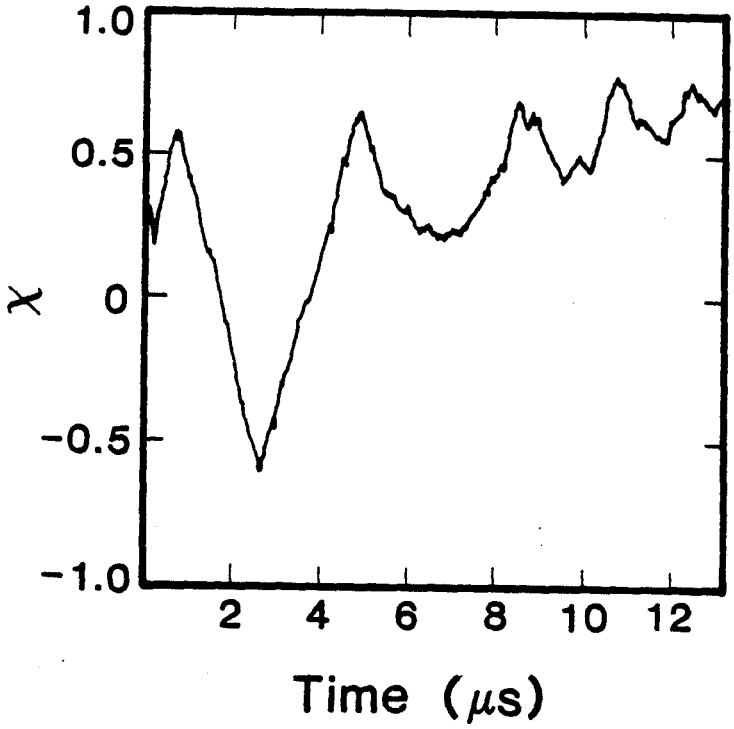

Figure 20

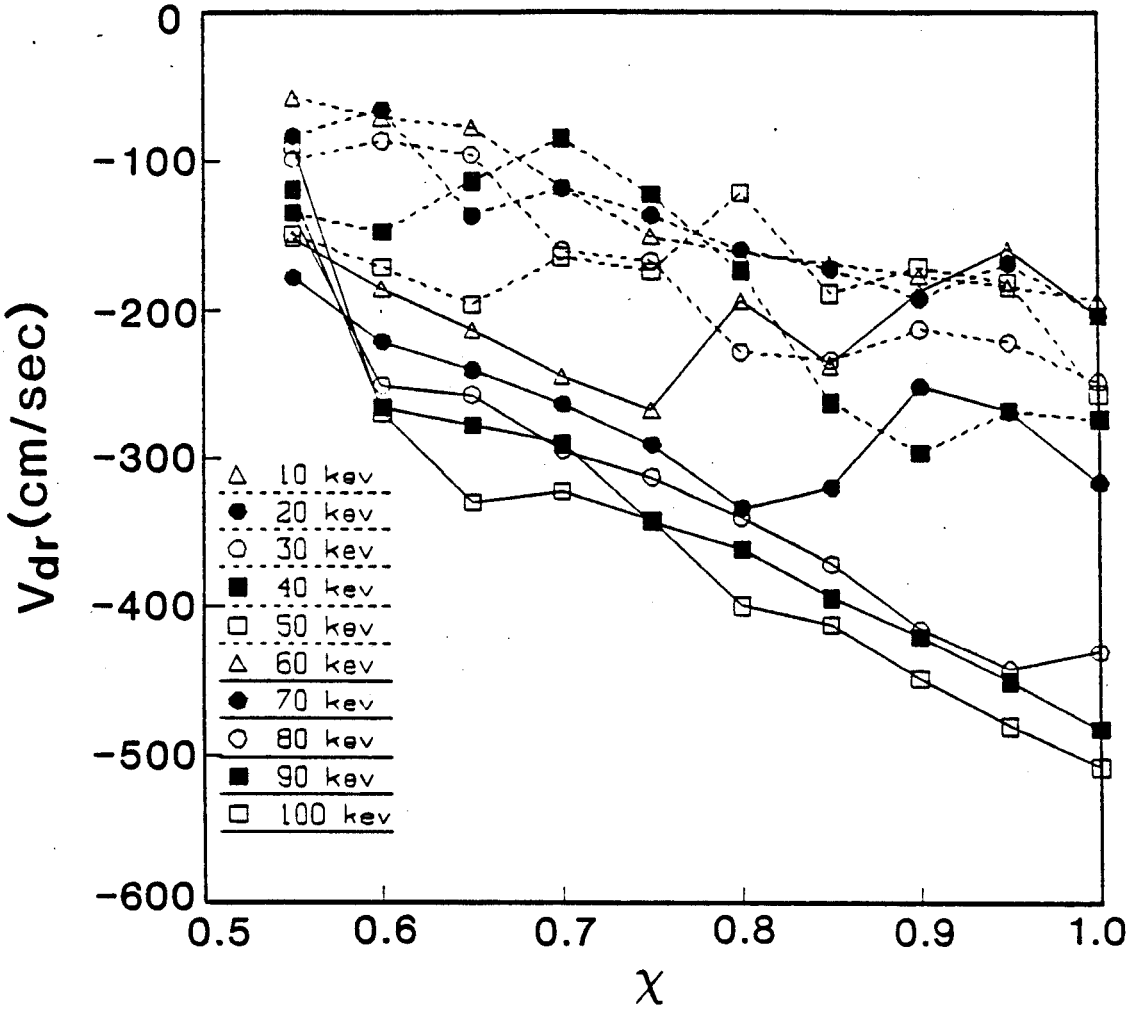
0
-100
-200
-300
-400
-500
-600
0.5
0.6
0.7
0.8
0.9
1.0
χ
V_{dr}(cm/sec)
10 kev
20 kev
30 kev
40 kev
50 kev
60 kev
70 kev
80 kev
90 kev
100 kev

Figure 21